

## Post-anthropogenic landscape evolution: Terrain reshaping and geomorphic response in the Loess Plateau<sup>☆</sup>

Liang Xue <sup>a,\*</sup>, Xie Hu <sup>b</sup>, QiuHong Tang <sup>c</sup>, Shengwen Qi <sup>d</sup>, Robert Moucha <sup>a</sup>

<sup>a</sup> Earth and Environmental Science Department, Syracuse University, New York, USA

<sup>b</sup> College of Urban and Environmental Sciences, Peking University, Beijing, China

<sup>c</sup> Key Laboratory of Water Cycle and Related Land Surface Processes, Institute of Geographic Sciences and Natural Resources, Chinese Academy of Sciences, Beijing, China

<sup>d</sup> State Key Laboratory of Lithospheric and Environmental Coevolution, Institute of Geology and Geophysics, Chinese Academy of Sciences, Beijing, China

### ARTICLE INFO

#### Keywords:

Landscape evolution model  
Soil erosion  
Infiltration  
Yan'an  
Loess Plateau

### ABSTRACT

Humans are altering Earth's surface at unprecedented scales due to rapid urban expansion. Here we investigate the long-term geomorphic consequences of large-scale anthropogenic landscape modification, focusing on a recent mountain excavation and city construction project in the Loess Plateau region of China. In this project, tens of square kilometers of urban region were newly constructed by mountain top removal and valley filling, significantly altering the region's topography. We applied a Landscape evolution model (LEM) to simulate future natural landscape dynamics, including the erosional stability, soil thickness, and landslide potential over the next one hundred years following this landscape alteration. Moreover, we evaluate the short-term impacts on the stage water height and infiltration, which is related to potential flooding risk during heavy rainfall events. Our results reveal that the altered landscape exhibits significant susceptibility to soil erosion, redistribution of soil thickness, and increased landslide potential, particularly along the margins of the newly constructed zones and at the outlet of the Yanhe River tributary. Perturbations in infiltration rates and runoff behavior are also observed during the rainy season. This study underscores the scientific potential of LEMs as predictive tools for understanding the long-term behavior of engineered loess terrains—environments that are highly sensitive to anthropogenic modification and hydrological variability. By capturing the coupled feedback between erosion, infiltration, and slope instability, the modeling framework offers a robust basis for forecasting geohazards in the context of rapid urban expansion. These findings not only support proactive hazard mitigation and infrastructure planning but also contribute to advancing theoretical frameworks in anthropogenic geomorphology. Continuous monitoring, integrated with model-driven land-use planning, will be essential for achieving resilient and sustainable development in highly engineered and geomorphically dynamic landscapes.

### 1. Introduction

Since the Mid/Late Holocene, land overexploitation has diachronously influenced topography in different parts of the world (e.g., [Ellis et al., 2013](#)). Population growth and urban expansion can further aggravate the tension between human and ecological environment, especially in naturally fragile environments (e.g., [Ehrlich and Holdren, 1971](#); [Moore, 2016](#)). The distribution of land cover is frequently modified due to increasing and shifting demands for urban development and changing land-use policy (e.g., [Allan et al., 2022](#); [Lambin et al., 2003](#); [Li et al., 2017](#)). Response of hydrology, soil, and biota to these spatially

complex and temporally dynamic landscapes depends not only on population growth, but more directly on human-induced terrain reshaping such as local slope change and anthropogenically produced land cover ([Stephens et al., 2021](#)). Large-scale terrain modifications—including mountain excavation, valley filling, slope cutting, and vegetation removal—are key drivers of instability in urbanizing landscapes. An anthropogenically unstable landscape may result in the loss of landscape functionality and productivity (e.g., [Maurer and Gerke, 2016](#)). Moreover, construction-driven drainage alteration and the formation of artificial gullies developed during urban expansion could cause deep incisions, rapid erosion, and further, water ingress into the

<sup>☆</sup> This article is part of a Special issue entitled: 'Deserts and Loess' published in Geomorphology.

\* Corresponding author at: Department of Earth and Planetary Sciences, University of California, Davis, CA, USA.

E-mail address: [lxue07@syr.edu](mailto:lxue07@syr.edu) (L. Xue).

strata, which may be subject to the exposure and transport of contaminated sediments/materials (Barnhart et al., 2020a). To alleviate the risks to local infrastructure and environment, an assessment of reformed landscape is required in terms of erosional instability and hydrology as an integral part of post-construction land-use plan.

While landscape evolution models (LEMs) are commonly used to study long-term interactions between tectonics, climate, and surface processes over thousands to millions of years, there is still no established framework for incorporating anthropogenic transformations—particularly large-scale urban expansion—into long-term landscape evolution predictions (e.g., Barnhart et al., 2020a). Current efforts have focused on forecasting landscape changes due to smaller-scale anthropogenic impacts, such as uranium mine tailings (Barnhart et al., 2020a; Hancock et al., 2015), tailing dams (Slingerland et al., 2018), and waste landfills (Neuhold and Nachnebel, 2011). Furthermore, uncertainties in dynamic variables like material properties, process rates, climate change, vegetation cover, and land management strategies add complexity, making it difficult to predict long-term landscape changes accurately. Addressing these issues is essential for advancing our understanding of how large-scale human activities will reshape future landscapes.

Here, we focus on the Mountain Excavation and City Construction (MECC) project in China's Loess Plateau, covering tens of square kilometers (Fig. 1). MECC project has provided a solution to address the growing challenge of increasing population and decreasing available land in the process of rapid urbanization (e.g., Wei et al., 2021). This mega-engineering project, initiated in 2012 to support urban expansion, aims to develop 78.5 km<sup>2</sup> of new urban area across the region's hilly

terrain to accommodate a rapidly growing metropolitan population (e.g., Juang et al., 2019). We refer to the “new urban area” as the region outlined in Fig. 1d. A total of 33 hilltops has been cut, and numerous incised valleys—some referred to as gullies in local planning documents—have been filled to create flat terrains, resulting in a change of local relief of 308 m and the construction area extended to 22.3 km<sup>2</sup> by 2015 (Hu et al., 2021). Such dramatic changes of the landscape would have an impact on local watercourses, vegetation, sediment flux, and channel and hillslope behaviors. Specifically, Loess materials are naturally subject to irregular wetting-induced compaction, which may lead to fractures in roads, infrastructures, pipelines, and possible catastrophic collapses (Li et al., 2018a, 2018b; Tabarsa et al., 2018; Wang et al., 2019). Thus, concerns about geohazards and water-related hazards in the distant future—which depend not only on the erosion rates of loess materials but also on land cover changes—demand a long-term (100 yr) projection of erosional stability and short-term (monthly) estimation of perturbation to the stage water height and infiltration. These anthropogenic landforms are not merely static platforms—they evolve over time through mechanical deformation, slope failures, and feedback with hydrological processes. Yet, the scientific understanding of their mid- to long-term behavior under natural forcing remains limited, especially in collapsible, erosion-prone loess environments (Juang et al., 2019; Zhou et al., 2022).

In this study, we investigate the geomorphic and hydrological consequences of large-scale anthropogenic terrain reshaping through the MECC project, where mountaintop removal and valley filling have drastically modified the loess landscape. The resulting artificial platforms, composed primarily of compacted Malan and Lishi Loess, are

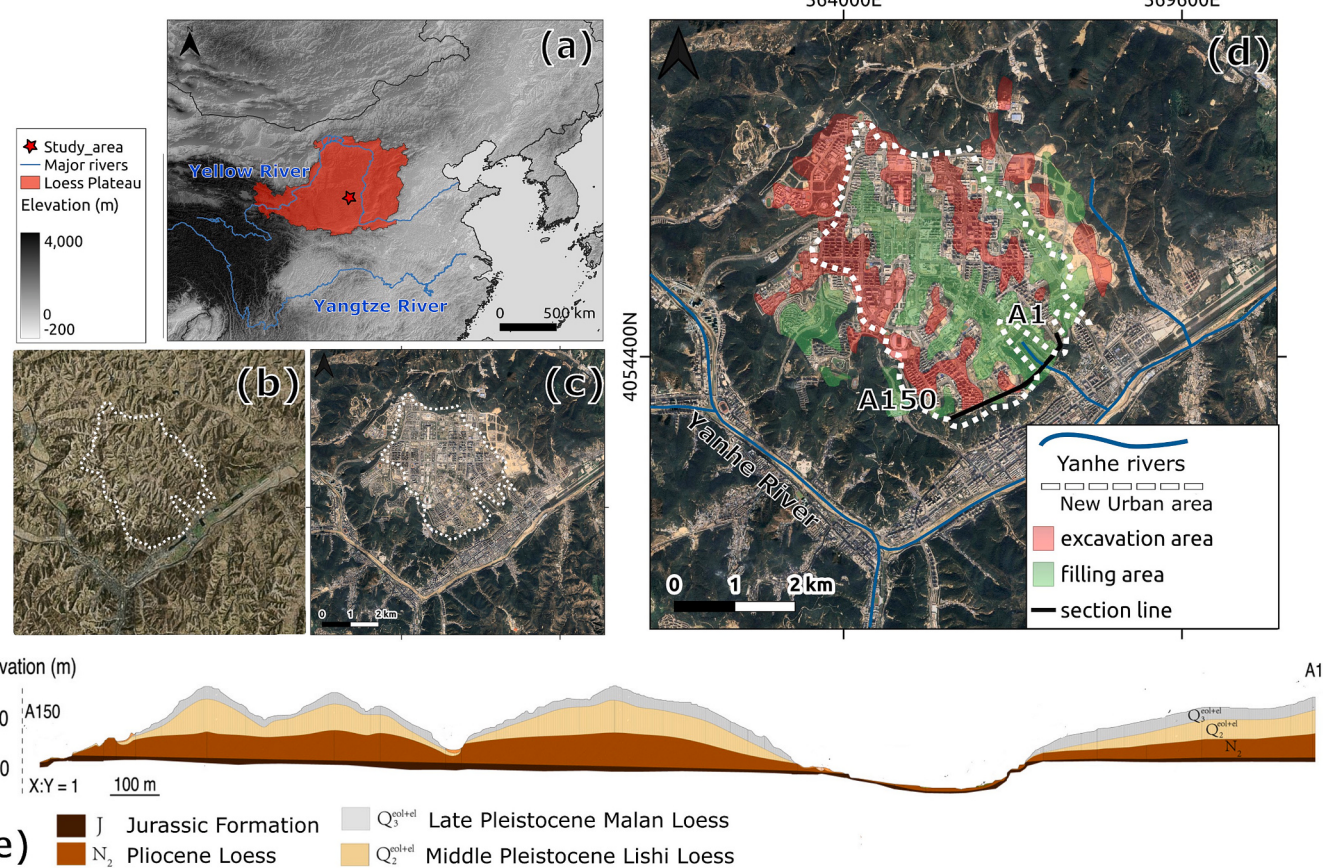


**Fig. 1.** (a) Regional map showing the location of Loess Plateau and the red star showing Yan'an region. (b) Pre- and (c) post-city construction optical satellite image of Yan'an region (2009 vs 2015). (d) Post-construction satellite image with the white dotted line outlines the new urban region. The green and red shades depict the filling area and excavation area, respectively (modified from Wu et al., 2019). A1 and A150 indicate the starting and end point of the cross section. (e) Geological cross section along the line section line A1-A150 shown in panel (d) from Hu et al. (2021), showing the elevation and stratigraphy prior to MECC.

highly sensitive to infiltration, erosion, and structural deformation, posing new challenges for long-term landform stability. To address these challenges, we pose the following research questions: (1) How does natural topography evolve under rainfall-driven erosion over decadal to centennial timescales following large-scale anthropogenic transformation? This is addressed through long-term simulation using a Landscape Evolution Model (LEM), which incorporates anthropogenic transformations alongside natural processes to capture soil depth changes, slope retreat, and surface deformation. (2) Where are the zones most vulnerable to landsliding and erosion, and how do these risks shift over time? We extract slope failure likelihood and erosion thresholds from spatial outputs of the LEM under different rainfall and material scenarios. (3) How does terrain modification alter short-term hydrological responses, such as infiltration rates and peak stage water height during storms? These hydrological dynamics are simulated at fine temporal resolution using infiltration and runoff modules embedded within the LEM framework. To answer these questions, we combine high-resolution digital elevation models, observed surface deformation data, and process-based modeling to quantify geomorphic and hydrological responses to engineered landform change. In this study, our emphasis is on the consequences of anthropogenic transformations, focusing on how natural surface processes respond to landscapes that have already been transformed. We distinguish our approach from studies that model the immediate effects of ongoing human activities. While LEMs have traditionally focused on natural drivers such as tectonics and climate, their application to anthropogenic terrains remains limited (e.g., Barnhart et al., 2020b). Our work extends the LEM framework to human-modified landscapes, offering predictive insights into erosion processes, terrain stability, and hazard potential in one of the world's most actively reshaped loess environments.

## 2. Geological background

### 2.1. Geology

Yan'an is situated in the southern part of the Loess Plateau, within the upper and middle reaches of the Yellow River in China (Fig. 1a). The area surrounding Yan'an has an average loess thickness of approximately 80 m, as determined from the loess thickness stratification map (Fig. 1e; Zhu et al., 2018; Wang et al., 2010).

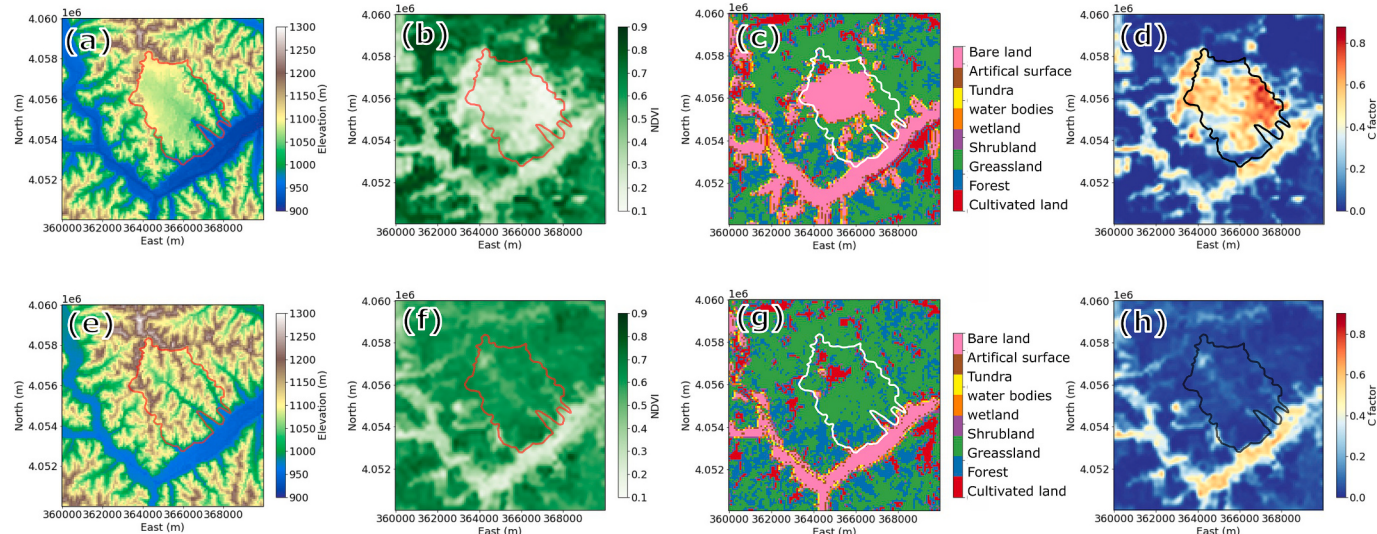


**Fig. 2.** Remote sensed data used for the LEMs. (a) post- and (e) pre-city construction DEM data from TanDEM-X DEM in 2015 and Shuttle Radar Topography Mission in 2000, respectively. (b) post- and (f) pre-city construction NDVI data from NASA MODIS-MOD13Q1 in 2018 and 2011. (c) post- and (g) pre-city construction land use information in 2020 and 2010 from GlobeLand30. (d) post- and (h) pre-construction cover and management factor (C-factor, see text) calculated from NDVI and land use information, used in erodibility calculation in the LEM. The solid line outlines the land-creation area from Pu et al. (2023), which could be slightly different from the outline in Fig. 1 (modified from Wu et al., 2019).

The Loess Plateau's original landscape features interwoven hills and gullies, with a stratigraphic sequence composed of Late Pleistocene Malan Loess at the surface, underlain by Middle Pleistocene Lishi Loess, and Neogene Pliocene at the bottom (Fig. 1e; Liu et al., 1987). Across the Plateau, loess thickness generally ranges from 0 to 350 m, with an average of around 106 m (Zhu et al., 2018). The surface Malan Loess is defined by its large voids (>50 % porosity), substantial water-bearing capacity, and collapsibility under self-weight, making it highly sensitive to water infiltration (Yang et al., 2022). This infiltration process increases the bulk weight of Malan Loess, reducing shear strength and often leading to shallow landslides along the loess slopes (Wang et al., 2015).

### 2.2. Climate and geohazards

The Loess Plateau of China has an arid to semi-arid climate with strong seasonality, where the winter is dry and windy, and summer is wet and hot, and spring and fall are short transition seasons (e.g., Chen et al., 2016). The elevation of Yan'an region ranges from 900 to 1300 m (Fig. 2a). The 24-hour average temperature ranges from  $-5.5^{\circ}\text{C}$  in January to  $23^{\circ}\text{C}$  in July (Xu et al., 2019). The annual precipitation total is about 450–650 mm with 70 % of the total annual precipitation received from June to September. The greatest rainfall intensity within a 24-h period was 139.9 mm in 1981, and the maximum rainfall was 577 mm in July 2013 (Xu et al., 2019). Given the relatively weak and steep loess slopes, seasonal rainfall may result in periodic landslides and even runout failures (Liu et al., 2020; Meng et al., 2021). About one-third of landslides in China occurred in the Loess Plateau (Juang et al., 2019), and Yan'an region has experienced several mass wasting disasters in the past. For example, the extreme rainfall in July 2013 resulted in more than 8000 landslides with 45 casualties (Wang et al., 2015). In the Yan'an region, most landslides are primarily shallow due to the limited infiltration depth, typically within a few meters' depth (Wang et al., 2015; Zhuang et al., 2017). These landslides can also cause further cascading geohazards of collapses and landslides related to soil erosion and environmental deterioration (e.g., Kou et al., 2020; Huo et al., 2020).

### 2.3. Geomorphological setting

Yan'an lies within the hilly and gully landscape of the central Loess Plateau, one of the world's most extensive and deeply dissected loess-covered regions. The region is characterized by a dense network of gullies, loess tablelands, and steep valley walls, shaped by prolonged fluvial incision, surface runoff, and eolian deposition. These geomorphic features result from a combination of tectonic uplift, Quaternary climatic oscillations, and loess accumulation processes, which have created a highly erodible terrain prone to mass movement and sediment transport (Leng et al., 2023). The valley systems, shaped by hydrodynamic and climatic factors, strongly control geomorphic evolution and hazard occurrence, especially in areas like Zichang County within Yan'an, where geomorphological controls are closely linked to landslide distribution and erosion processes (Zeng and Huang, 2010). The region's high ecological vulnerability, influenced by slope aspect, vegetation cover, and land use practices, also plays a pivotal role in driving soil loss and gully expansion (Hou et al., 2016).

### 2.4. Mountain Excavation and City Construction (MECC)

The MECC project in Yan'an exemplifies an unprecedented scale of anthropogenic landscape transformation in a loess-dominated terrain. This mega-engineering initiative, launched in 2012, aimed to reshape the naturally rugged hill-gully system of the central Loess Plateau into flat terraces suitable for urban development. This involved initially modifying the land surface to the west of the city, subsequently extending the alterations eastward (e.g., Hu et al., 2021). Approximately 10.4 km<sup>2</sup> of ridges were excavated and 12.3 km<sup>2</sup> of adjacent valleys were filled, involving the movement of nearly 490 million m<sup>3</sup> of earth (Wu et al., 2019). The geomorphic effect of this intervention is profound: natural drainage networks have been disrupted, local relief drastically reduced, and slope dynamics fundamentally altered.

The artificial platforms created during MECC rely heavily on compacted loess—primarily Malan and Lishi strata—as fill material. Although mechanically densified during construction, SEM analyses reveal that the reworked loess matrix exhibits diminished structural cohesion due to crushed particle interfaces and increased pore space (Ma et al., 2020). InSAR-based surface deformation monitoring from 2015 to 2019 confirms that these filled zones are undergoing significant post-construction subsidence—up to 87 mm/year in some areas—while excavated zones often show rebound-related uplift, driven by stress redistribution and loess collapsibility (Zhou et al., 2022). These changes highlight the inherent instability of remolded loess and the geomorphic implications of large-scale terrain reshaping.

Hydrologically, MECC-induced topographic changes have altered surface runoff patterns, subsurface infiltration pathways, and slope saturation regimes. The reduction of natural slope gradients and burial of gullies has led to the formation of poorly drained zones, increasing the risk of waterlogging and delayed saturation of filled loess. Rainfall-induced pore pressure build-up in these materials—already prone to collapse upon wetting—can initiate shallow slope failures and ground settlement, especially during the monsoon months (Leng et al., 2023; Cao et al., 2024). Furthermore, MECC disrupts subsurface water redistribution, exacerbating hydrogeological imbalances and increasing vulnerability to localized piping and erosion—a well-known hazard in loess terrains (Juang et al., 2019).

In terms of broader geomorphological impacts, the engineered flattening of the hill-gully system eliminates critical microtopography responsible for moderating sediment transport, slope stability, and vegetation dynamics. Field studies indicate that up to 60 % of post-construction subsidence occurs within fill areas, while over 65 % of uplift is concentrated in cut zones, demonstrating a spatial asymmetry in landform response (Wu et al., 2019). These landforms also evolve through time due to seimi anthropogenic processes; fill zones may settle unevenly depending on compaction efficiency, material moisture

content, and depth, leading to differential deformation and geotechnical instability of overlying infrastructure (Zhou et al., 2022).

Ultimately, the MECC project in Yan'an serves as a striking case study in anthropogenic geomorphogenesis, demonstrating how large-scale earth reshaping in fragile loess landscapes creates a new generation of geomorphic systems with distinct hydrological behaviors, mechanical instabilities, and evolving hazards (Juang et al., 2019; Cao et al., 2024). These engineered landforms require continuous monitoring and adaptive management to mitigate future geohazards and maintain urban stability.

## 3. Methods

### 3.1. Landscape evolution model

To evaluate the impacts of anthropogenic transformation on landscape evolution, we used the LEM Landlab, an open source, python-based landscape evolution library (Hobley et al., 2017; Barnhart et al., 2020b; Hutton et al., 2020). Landlab is a toolkit designed for simulating Earth surface processes using a grid-based structure and finite-difference numerical methods (e.g., Hobley et al., 2017; Barnhart et al., 2020a). It operates on a raster or hexagonal grid where topographic elevation and other fields (e.g., soil depth, water discharge) evolve over time according to user-defined physical processes. Each process is implemented through independent components that can be flexibly combined to model complex interactions between hydrology, sediment transport, and tectonics (Shobe et al., 2017). In our study, we coupled key components including Space, Flow Accumulator, DetachmentLtdErosion, DepthDependentDiffuser, and InfiltrationGreenAmpt to simulate overland flow routing, detachment-limited erosion, soil creep, and dynamic infiltration, respectively (Fig. 3). These components exchange field data at each timestep, allowing the model to simulate coupled feedback across geomorphic and hydrologic domains. By assembling this component suite, we are able to reproduce both short-term hydrological responses and long-term erosional behavior over engineered loess terrain, while retaining flexibility to modify input parameters and process combinations as needed.

The Landlab component SPACE (Shobe et al., 2017) was used for erosion and deposition analysis. In this model, the conservation of sediments follows the erosion/deposition approach of Davy and Lague (2009), and the spatial change in volumetric sediment discharge  $Q_s$  per unit width ( $w$ ) is given by:

$$\partial(Q_s/w)/\partial x = E_s + (1 - F_f)E_f - D_s \quad (1)$$

where  $E_s$  and  $D_s$  are the volumetric entrainment flux and deposition flux per unit bed area, respectively. The  $E_f$  is the volumetric erosion flux of bedrock per unit bed areas.  $F_f$  is a nondimensional fraction of fine fluvial

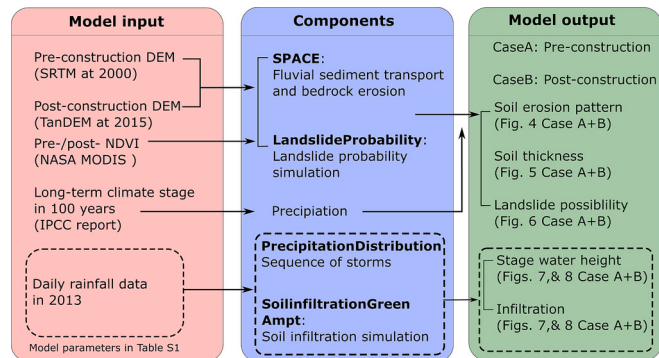


**Fig. 3.** Workflow chart of the landscape evolution model and its components used in this study. The dashed box represents the processes involved in short-term modeling simulation.

sediment, the factor  $1-F_f$  represents a fraction of bedrock particles detached from the bed that are small enough to stay as permanent suspension and not be tracked as bed sediment. Note that all the parameter values are listed in Table S1 and workflow is shown in Fig. 3. The sediment entrainment and bedrock erosion are governed by the stream power law (e.g., Whipple and Tucker, 1999). Here  $E_s$  and  $E_f$  are modified from the ratio of bed sediment thickness  $H$  to reach-scale bedrock roughness length scale  $H'$ , i.e.,  $H/H'$ . Either a large bed sediment thickness or a low bedrock surface roughness would result in a small bedrock exposure to erosive flows. SPACE assumes an exponential increase in sediment entrainment rate with the increase of  $H/H'$  and use the rate to distinguish cases with sediment entrainment (Shobe et al., 2017), hence the rates of sediment entrainment and bedrock erosion can be written in the form of stream power law as:

$$E_s = (K_s q S^n - \omega_{cs}) (1 - e^{-H/H'}) \quad (2)$$

$$E_f = (K_r q S^n - \omega_{cs}) (1 - e^{-H/H'}) \quad (3)$$

where  $K_s$  and  $K_r$  are the erodability efficiency for sediment and rock, respectively, that include lithology erodibility.  $S$  and  $n$  are local slope and empirical exponent (generally  $n = 0.5$ ).  $\omega_{cs}$  is a threshold of stream power needed for sediment entrainment.  $q$  is the water discharge per unit channel width and can be simplified as  $q = K_q P A^m$ , where  $A$  and  $m$  are drainage area and empirical exponent (generally  $m = 1$ ), and  $K_q$  can be subsumed into  $K_s$  and  $K_r$ .  $P$  is the precipitation factor that scales precipitation based on climate scenarios. In addition to water erosion based on stream power, we added hillslope soil transport using a simplified linear diffusion model:

$$\text{elevation}/\partial t = d\nabla^2 \text{elevation} \quad (4)$$

where  $d$  is the diffusion coefficient (e.g., Shobe et al., 2017).

The DEMs pre- and post-construction are from TanDEM-X DEM in 2015 and Shuttle Radar Topography Mission in 2000, respectively, and discretized with a horizontal cell spacing of  $\sim 90$  m (3 arc sec) in both directions. We conduct simulations across two distinct time scales: The evaluation of erosion stability, sediment thickness, and landslide potential spans one hundred years. Meanwhile, the assessment of stage water height and infiltration occurs over a shorter time scale of three months. Subsequent sections and Table S1 will provide detailed insights into these two simulation approaches.

### 3.2. Long-term erosion and landscape evolution

Tectonic uplift and climate are the dominant external drivers for the long-term landscape evolution. Here we assume that there is no change in base level or tectonic uplift, nor fluctuations in water level of catchment outlet over a centennial timescale. Hence, the climate would be the predominant cause of erosion, sediment transportation, and deposition across the post-MECC landscape. For long-term climate (precipitation) change, we consider three scenarios with an increase of precipitation by 0 %, 25 %, and 50 % to represent three climate stages. Here we consider an increase in precipitation is based on the Intergovernmental Panel on Climate Change (IPCC) report on the long-term climate change projection (Collins et al., 2013). Multiple models suggested an increase of 30–50 % of precipitation in the region of Loess Plateau in 2081–2100 relative to 1986–2005 CMIP5 models (Collins et al., 2013).

Changes in land usage induced by human activities can influence surface processes. In this study, we utilize land use data and the Normalized Difference Vegetation Index (NDVI) to derive the C-factor (cover management factor; e.g., Panagos et al., 2015; Alexandridis et al., 2015). C-factor serves as a proxy for scaling surface erosion risks under the influence of vegetation coverage, which is given by:

$$K_s = K^* C$$

$$C = \exp\left(\frac{-a^* NDVI}{b - NDVI}\right) \quad (5)$$

where  $a$  and  $b$  are constants that determine the shape of the NDVI-C curved, derived from a similar work in Loess Plateau (Chen et al., 2021). This application quantifies various land use categories, for instance, a low C-factor aligns with forested regions, while a relatively higher C-factor is associated with vineyards (e.g., Panagos et al., 2015; Cossart et al., 2020). The estimated C-factor is used to modulate  $K_s$  and  $K_r$  in Eqs. (2) and (3) as a percentage following the method of Chen et al. (2021). Note that both of the sediment and bedrock effective erodibility coefficient ( $K_s$  and  $K_r$ ) are modified by C-factor while the bedrock in the model has a lower base (Table S1). The NDVI data, featuring a spatial resolution of 250 m, was retrieved from NASA's MODIS dataset for the years 2011 and 2018, representing the pre- and post-MECC periods, respectively (source: [modis.gsfc.nasa.gov/data/dataproducts/mod13.php](http://modis.gsfc.nasa.gov/data/dataproducts/mod13.php)). Concurrently, land use data for the years 2010 and 2020 was sourced from GlobeLand30 with a spatial resolution of 30 m (source: [www.globallandcover.com](http://www.globallandcover.com)).

Significant topographical changes, exemplified by events like MECC, have the dual impact of not just influencing local surface processes but also altering slope processes, thereby influencing the potential for landslides (e.g., Keles and Nefeslioglu, 2021; Strauch et al., 2018). Here, we adopt a Landlab component, LandslideProbability (Strauch et al., 2018), to simulate slope failure where the factor of safety (FS) for an infinite slope stability and probability of failure is given by:

$$FS = \frac{(C_r + C_s)/h_s \rho_s g}{\sin\theta} + \frac{\cos\theta \tan\phi (1 - R_w \rho_w / \rho_s)}{\sin\theta} \quad (6)$$

$$P(F) = P(FS \leq 1) = nP(FS \leq 1)/N \quad (6)$$

where  $C_r$  and  $C_s$  are the root and soil cohesion, respectively,  $h_s$  is the soil depth perpendicular to slope and  $R_w$  is the ratio of subsurface flow depth and the soil thickness is the ratio of subsurface flow depth to soil thickness, which depends on contributing area, local soil transmissivity, and recharge rate.  $\rho_s$  and  $\rho_w$  are the wet soil and water density, respectively,  $\theta$  is the slope angle,  $g$  is standard gravity, and  $\phi$  is the internal friction angle of soil (e.g., Hammond, 1992). The initial soil thickness in the model is 2 m from Wang et al. (2010). The function  $n$  and bracket count the number of conditions satisfied within the brackets, and  $N$  represents the number of iterations. In this component, Eq. (6) is solved using a Monte Carlo method with 1000 iterations, where the probability of failure is computed for each grid cell under the condition  $FS \leq 1$ .  $P(F)$  gives the relative likelihood of landslide initiation in each grid cell. Other parameters, such as slope, drainage area, and soil depth, are directly derived from LEM outputs. Other parameters (i.e., slope, drainage area, soil depth) are directly inferred from LEM results. We emphasize that this is not a dynamic landslide process model; it does not simulate mass movement or material transport during failure events. Instead, it employs a probabilistic slope stability model based on infinite slope theory, evaluating the factor of safety across grid cells to identify locations where shallow landslides are statistically likely to occur.

### 3.3. Short-term stage water height and infiltration

In addition to studying the long-term effects of land use changes over centuries as discussed above, it is equally important to understand the short-term impacts on processes like runoff and infiltration which is closely related to water-related hazards. Simulating these immediate effects provides some insights into how the landscape and hydrological systems respond to rainfall events after the MECC. Specifically, weather generators that can simulate gridded precipitation are often applied to study climate change impacts on hydrological responses (e.g., Peleg et al., 2017; Singer et al., 2018). We used the Landlab component *PrecipitationDistribution* to simulate one month of random uniform storms

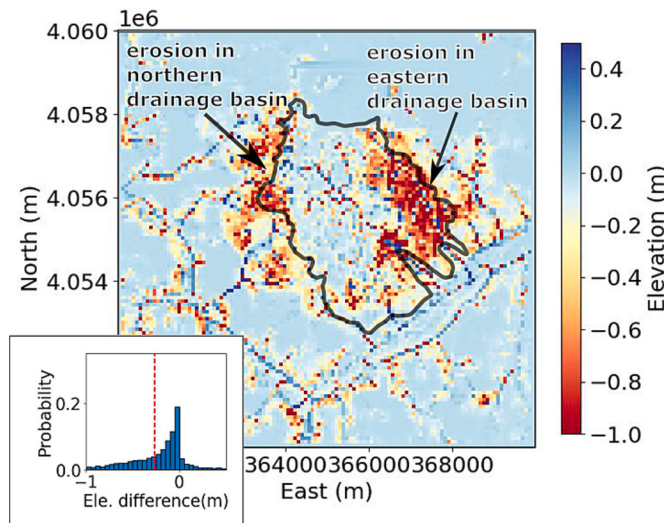
across the study area. Based on daily rainfall data from 2013 in Yan'an (Table S2), January and July intensities were selected to represent dry and rainy months, respectively. The monthly rainfall amount is 2.1 mm in January and ~ 560 mm in July from observation at station Baoshan in Yan'an city. Landlab component *PrecipitationDistribution* generates a sequence of storms over the study area using stochastic methods (Singer et al., 2018). The two random generated storms scenarios with time-dependent (hourly) rainfall intensity were applied to the LEM to estimate stage water height and infiltration. These storm-generated water fluxes contribute to the stage water height, representing the water level above the ground surface at the model's start for a given location. This stage water also infiltrates into the soil, estimated using the Landlab component, *SoilInfiltrationGreenAmpt* (Rengers et al., 2016; Campforts

et al., 2021), which tracks the depth of infiltrated water over time using the Green-Ampt method:

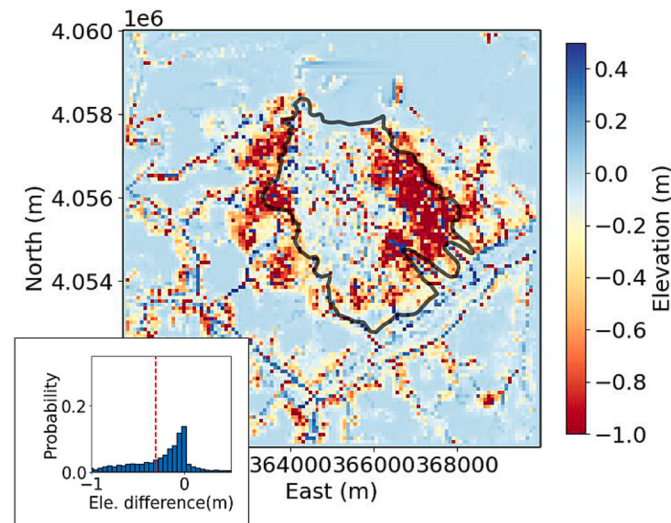
$$\text{infiltrationrate} = K_{sh} \left( 1 + \frac{(h + \Psi)(\phi_p - \theta_i)}{F} \right) \quad (7)$$

where  $K_{sh}$  is the saturated hydraulic conductivity,  $\phi_p$  is the porosity,  $\theta_i$  is the initial soil moisture content,  $F$  is the total infiltrated depth, and  $\Psi$  is the capillary pressure head at the wetting front (Green and Ampt, 1911). Here we determine  $\Psi = 0.04$  and  $\phi_p = 0.47$  for the soil type silt (Rawls et al., 1992). The  $K_{sh}$  of loess is from  $1.0 \times 10^{-9}$  to  $2.0 \times 10^{-5}$  m/s based on study of Domenico and Schwartz (1997), and we opt to an average of  $1.0 \times 10^7$  m/s for  $K_{sh}$  in the model. The stage water head ( $h$ ) is resolved

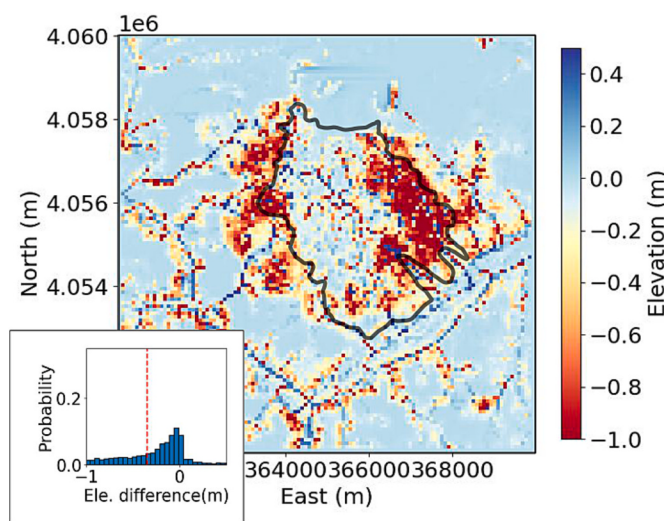
(a) elevation difference with a precipitation change of 0%



(b) elevation difference with a precipitation change of 25%



(c) elevation difference with a precipitation change of 50%



(d) elevation difference without construction

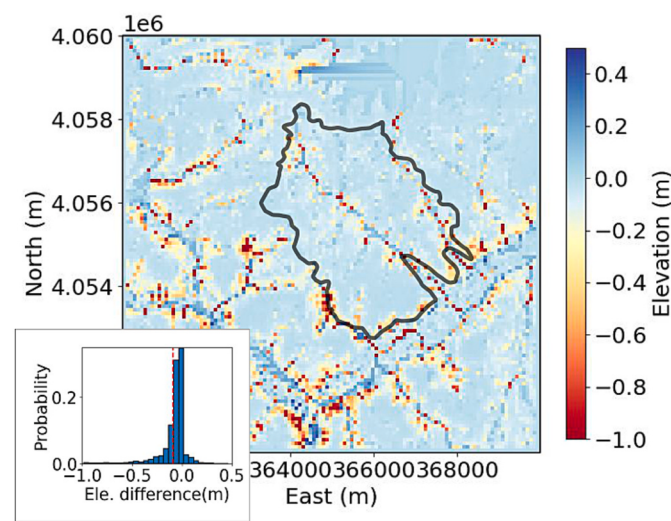


**Fig. 4.** Differential topography between initial topography and LEM results by the end of 100 yr with an increase of precipitation of 0 % (a), 25 % (b), and 50 % (c), representing variation in climate. (d) Differential topography between initial topography and LEM results without construction. Elevation difference is between the modeled elevation 100 years after construction and the present-day elevation (post-MECC). The positive and negative values indicate deposition and erosion respectively. The inset histograms show the elevation difference after 100 yrs. in the new urban region with the mean value shown as the dashed line. The black outlines the land-creation area from Pu et al. (2023).

from LEM model and the output is the total infiltrated depth ( $F$ ).

## 4. Results

### 4.1. Soil erosion

The LEM simulated soil erosion results are depicted as maps of differential topography between initial topography and the one after 100 yr with different precipitation representing three climate scenarios (Fig. 4). We found most erosion is concentrated along the margins of the new urban region where steep slopes and local low-relief valleys are located. Maximum erosion ( $\sim 1$  m) occurs in the region that was the outlet of the Yanhe watershed before construction. Such high erosion is probably due to the imposed headward incision of Yanhe River. Compared to the scenario without construction (Fig. 4d), the incision

along mainstream of Yanhe River to the south of the city is the same after the construction. Nevertheless, the northern and eastern drainage basin in the city new urban region experiences more erosion after construction (arrow in Fig. 4a). Particularly, for the channel of Yanhe River in the new urban region that has been totally filled, the new and smaller drainage would form in the margins of the new urban region and contribute to adjacent existing rivers and increase the erosion there.

We also observe certain influence of climate on post-construction erosion. Increasing precipitation yields more erosion in the new urban region. When the precipitation increase is 0 %, the mean erosion by the end of 100 yr is 0.27 m, while the precipitation increases to 50 % would result in a mean erosion of 0.35 m, suggesting an increase of 23 % (Fig. 4c). Within the new urban region, a wider area would be eroded  $>0.5$  m with increase of precipitation rate (Fig. 4 inset histogram).

The LEM simulated soil depth distribution presents a similar pattern

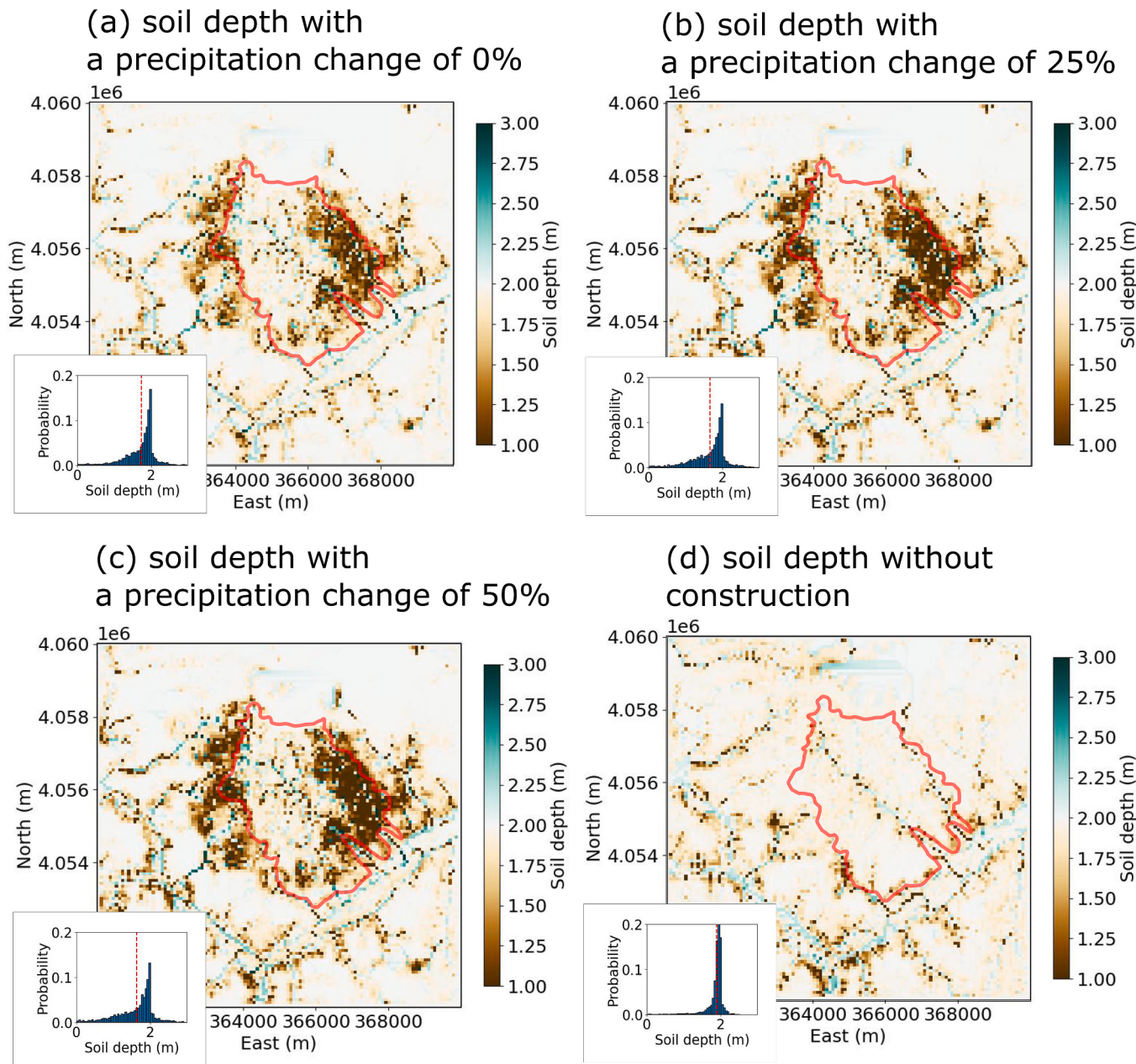


**Fig. 5.** Map of LEM simulated soil depth with an increase of precipitation of 0 % (a), 25 % (b), and 50 % (c), representing different levels of climate change. (d) LEM simulated soil depth without construction. The inset histogram shows the soil depth within the new urban area with the mean value shown as the dashed line. The red region outlines the land-creation area from [Pu et al. \(2023\)](#).

to erosion (Fig. 5). The marginal new urban of bare land (Fig. 2c) will experience the most erosion with the least soil depth remained (<1.5 m) with city construction. On the other hand, the Yan'an new urban region would be less eroded (Fig. 4d) without construction, and thus a soil depth (~2 m) would be preserved at the city region (Fig. 5d). The most eroded region will be the tributary gullies of Yanhe River. Moreover, an increase of precipitation results in less soil staying in the new urban region according to the projection of soil depth distribution (Fig. 5).

#### 4.2. Landslides

The modeled probability of the failure of shallow landslides is shown in Fig. 6. Post-construction landscape in the city's new urban region exhibits more failure potentials (Fig. 6a) than that from the non-construction scenario (Fig. 6b). It should be emphasized that the LandslideProbability component used in this analysis does not simulate landslide erosion processes or dynamics; rather, it is a statistical model that estimates susceptibility based on infinite slope stability theory. The modeled results suggest that steep surface that is devoid of vegetation or buildings (Fig. 2c) in the northeast and west of the new urban region is highly unstable. Such distribution of high failure probability corresponds to a low cohesion, here represented by the C-factor (Fig. 2d). These regions in the margin of the new urban have steep slopes and extended slope lengths than that of the undisturbed landscape. Notably, although the NDVI decreases over the bare earth within the new urban region, the slope steepness and length are reduced due to flattening, and thus the failure probability is relatively low in the center of the new urban region. In contrast, its margin presents a steep slope and low NDVI, therefore, presenting a higher failure probability.

#### 4.3. Short-term stage water height and infiltration

We also apply LEM for a short time span to assess the impact of MECC on stage water height and infiltration (Fig. 7). The time series of rainfall intensity in rainy and dry months is shown in Fig. 8, generated based on in-situ observations (Table S2). The modeled maximum rainfall intensity in the rainy month is about three times that in the dry month (Fig. 8). The stage water height and infiltration maps show that the rainy month has much higher stage water height and infiltration depth than those in the dry month (Fig. 7). Compared to the initial stage, the water height and cumulative infiltration depth occurs in the rainy month and can reach 25 m and 2.5 m (Fig. 7a, b). Such high values occur only at the

outlet of the new urban catchment, where the northern tributary of the Yanhe River was obstructed by massive loess infill during city construction (shown in Fig. 7a). This filling procedure creates a pit in stream profile along the channel and could be responsible for the anomaly in high stage water height in the rainy month. Within the new urban region, the stage water height is rather low because there are few water drainage pathways in such infilled and flattened area based on the observation from digital elevation models. The hydrological conditions of the non-construction scenario are also calculated as a reference to post-construction scenario (Figs. 7e, f and 8e, f). In the non-construction scenario, there will be no perturbation of elevation gradients around the new urban, therefore, the stage water height and infiltration will not concentrate at the infilled river valley, rather, stage water height is distributed across the upstream non-constructed catchment.

At the southern edge of the new urban area (Fig. 7a), which used to be the outlet of the original drainage basin, the outflow hydrographs show that the peak flowing depth is 0.06 m in the dry month and 37 m in the rainy month (Fig. 8), corresponding to the lowest (2 mm/h) and highest rainfall intensity (8 mm/h) of the month. During the dry month, the water level drops to zero within a few days after the rain (Fig. 8a). In contrast, during the rainy month, the high-water stage persists until the end of the period due to the combination of intense rainfall and low soil infiltration capacity (Fig. 8b). The cumulative infiltration depth at the same outlet can increase by 0.05 m and 0.4 m for dry and rainy months, respectively (Fig. 8). In the non-construction scenario, the water stage also remains high after the rainfall intensity peak, but it drops faster than that of the post-construction scenario (Fig. 8d).

## 5. Discussion

### 5.1. Soil erosion

The erosion rate in the new urban region of this anthropogenically modified landscape has changed in the spatial distribution (Figs. 4 and 5). The critical question here is how the predicted results in erosion and deposition compare to observations in the past. Therefore, we first validate the projected results with previous studies (e.g., Fu et al., 2011). Fu et al. (2011) suggested a soil erosion rate of  $500\text{--}2500 \text{ t km}^{-2} \text{ yr}^{-1}$  in Yan'an region from 2000, and 2008. Meanwhile, Zhao et al. (2013) also estimated sediment yield from erosion in 1955–1969 and 2000–2009 and reported that the soil sediment yield of  $\sim 5000\text{--}8000 \text{ t km}^{-2}$  and  $2500\text{--}5000 \text{ t km}^{-2}$ , corresponding to an average of 464 and 417  $\text{t km}^{-2}$

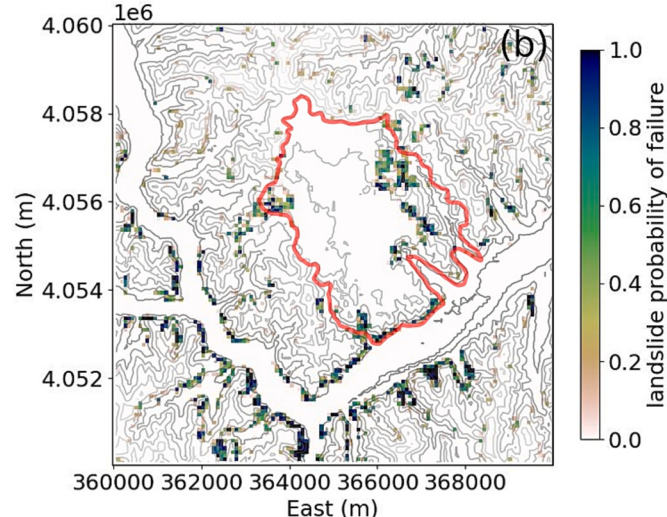
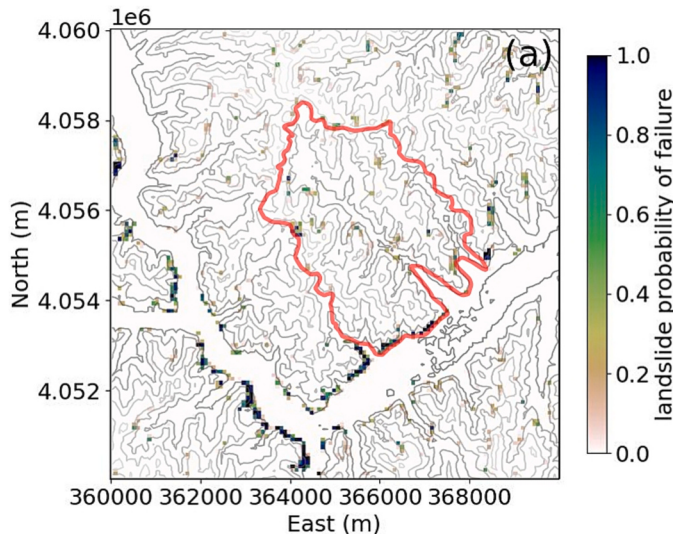


**Fig. 6.** Landslide probability of failure for the scenarios with no construction (a) and with post-construction (b). The background contour map is from topography with an interval of 50 m. The red region outlines the land-creation area from Pu et al. (2023). The contour map, derived from DEMs in Fig. 2, illustrates the slope gradient.

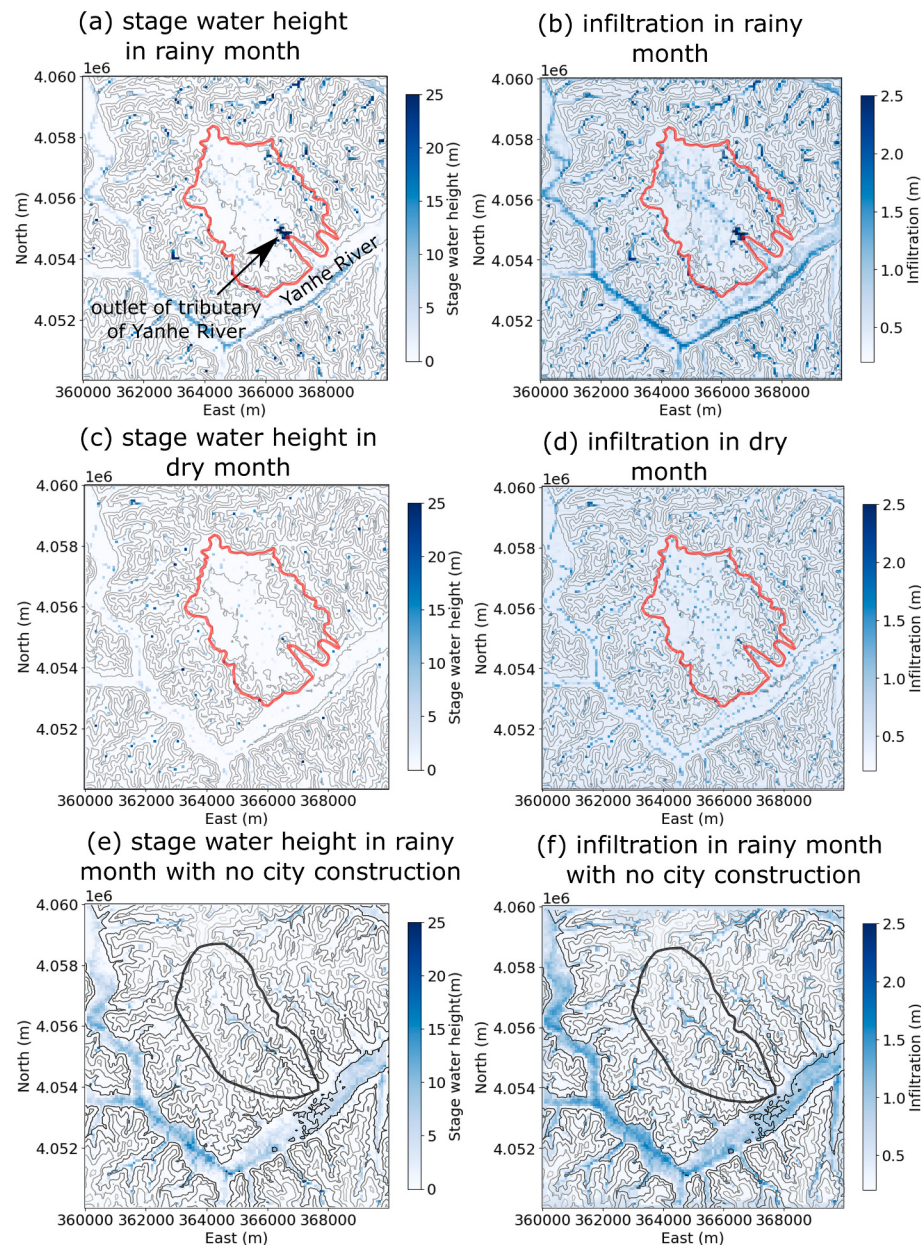


**Fig. 7.** Map of the highest stage water height and cumulative infiltration in rainy month (a and b), dry month (c and d) after city construction, and in the scenario with no city construction in the rainy month (e and f). The background contour map is from topography with an interval of 50 m, derived from DEM in Fig. 2. The location of Yanhe River and its tributary is shown in (Fig. 1d). The red region outlines the land-creation area from Pu et al. (2023). The black region outlines the catchment of the tributary of Yanhe River.

$\text{yr}^{-1}$  respectively. Our modeling results estimate a mean erosion in the new urban area of  $477 \text{ t yr}^{-1}$  without city construction over the next 100 years (Fig. 4d) when assuming a loess density of  $2650 \text{ kg/m}^3$ , which is comparable to these previous studies. This alignment between the modeled results and observations offers a degree of confidence in using LEMs as a tool to assess soil erosion and approximate the distribution of erosion following construction.

Considering models with forecasted increase in precipitation, we project extensive soil will be eroded from the flat surface of the new urban region into the canyon (Figs. 4, 5, and 9). An increase in precipitation of 25 % and 50 % would result in a total erosion increase of 16 % and 23 %, respectively. To evaluate long-term effect of the city construction, beyond IPCC projections, we extend the model time to 1000 years. Notably, the projected erosion varies with time, where the erosion rate without precipitation increase is  $\sim 0.03 \times 10^6 \text{ m}^3/\text{yr}$  at the first 100

years, then reduces to  $\sim 0.012 \times 10^6 \text{ m}^3/\text{yr}$  then (Fig. 9). In the catchment of the city's new urban region, total soil erosion in 1000 year is about 16 million  $\text{m}^3$ , which is twice as that from the case with no city construction (Fig. 9). This excess sediment delivery and erosion will continue until the landscape erodes to a lower slope or with vegetation establishment, assuming no human intervention/mitigation in this region.

Soil erosion is a critical factor in determining the long-term stability of landscapes, particularly for ecological sustainability, as it reflects the continuity of geomorphological processes. In the Yanhe River basin, soil erosion plays a dominant role in reshaping the region's topography and river systems within the Loess Plateau. For instance, the Dongzhiyuan highland, the largest in the Loess Plateau, contributes approximately 1.6 billion tons of eroded soil and silt to the Yellow River annually (Li and Sheng, 2011). The Yanhe River, a key tributary of the Yellow River, faces

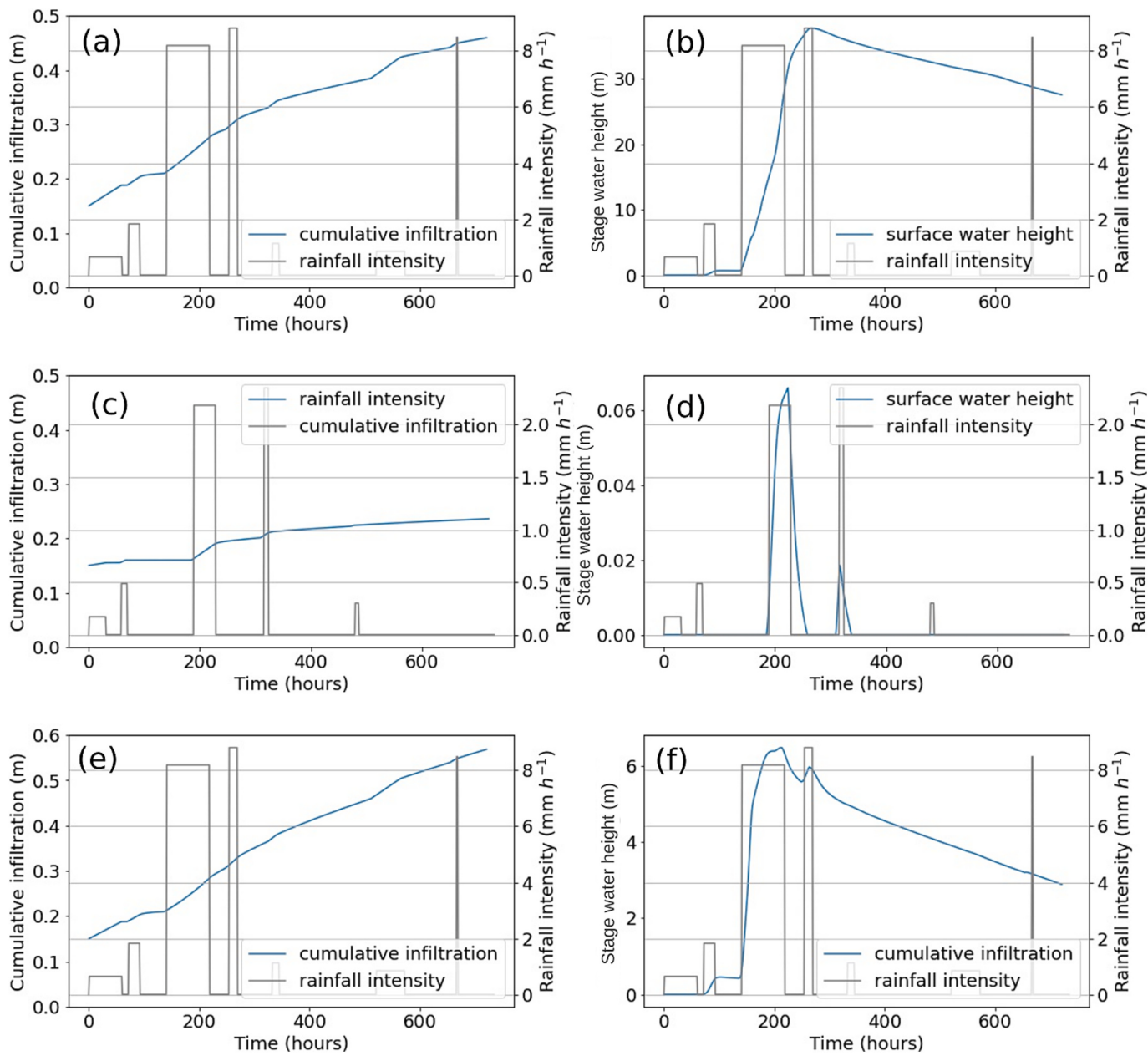


**Fig. 8.** Time series of cumulative infiltration and stage water height in the rainy month (a and b), dry month (c and d) after city construction, and in the scenario with no city construction in the rainy month (e and f). The blue and black curves represent stage height/infiltration and rainfall intensity respectively. All the data is collected at the location of the new urban catchment outlet (location shown in Fig. 7a). The right and left panel represents cumulative infiltration and stage water height respectively.

similar erosion pressures, with its discharge and sediment load highly influenced by regional soil erosion. Our model indicates that recent city construction has altered valley morphology and slope profiles, generating new knickpoints—steep breaks in the river gradient—that are likely to migrate upstream (i.e., headward erosion) into the newly urbanized areas over the next 100 to 1000 years (Fig. 10a). These evolving knickpoints signal enhanced erosion potential and highlight long-term implications for both landscape development and infrastructure resilience in urbanized loess terrains.

In addition to terrain changes, erosion is projected to increase in areas where significant differences in pre- and post-construction NDVI are observed (Fig. 2b & f). Vegetation's role in mitigating erosion rates is well-established (e.g., Duzant et al., 2011), but in this context, vegetation coverage serves as a secondary impact. While our models do not account for city infrastructure or vegetation restoration plans (see

Section 5.5 for limitations), the introduction of vegetation buffering zones on the steepest slopes and newly filled valleys could help mitigate the projected increase in erosion (e.g., Hancock et al., 2017). Implementing these strategies could be critical for minimizing erosion while ensuring long-term landscape stability.

## 5.2. Landslide potential

The high sensitivity of loess to water makes the Loess Plateau especially vulnerable to landsliding (e.g., Ma et al., 2020). Please note that our modeled results represent probabilistic assessments of shallow landslide susceptibility, not dynamic simulations of landslide movement. The results suggest the newly constructed urban area has introduced steepened slopes at its margins, which, combined with sparse vegetation and low soil cohesion, drive higher failure potential in these

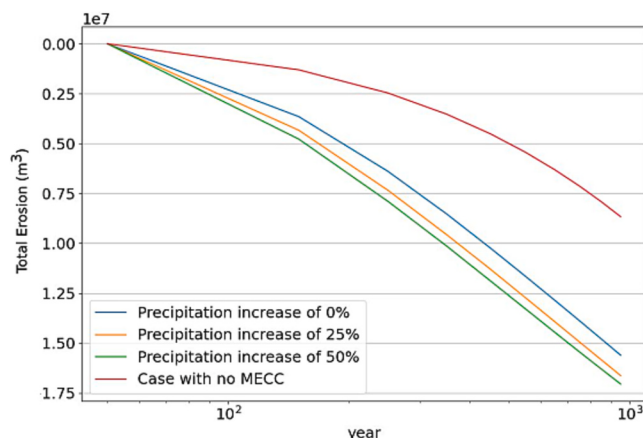


**Fig. 9.** Whole basin total erosion from 0 to 1000 years, showing the scenarios with an increase of precipitation of 0 %, 25 %, and 50 %, and the one with city new urban construction. The basin covers all the new city district region.

zones (Fig. 6). For example, the slope gradient along the Yanhe River increased after the construction, contributing to instability at the urban edges. This pattern aligns with areas of low NDVI and high erosion risk, reinforcing the importance of terrain reshaping in influencing landslide susceptibility. These modeled high-risk zones correspond with InSAR-derived surface deformation observations (Pu et al., 2023), and field data show similar instabilities linked to rising groundwater levels (Juang et al., 2019). Hydrological processes such as precipitation and irrigation—though vital for vegetation restoration—can exacerbate slope failure in loess terrain, particularly when infiltration increases pore water pressure on artificial slopes (e.g., Derbyshire et al., 2000; Xu et al., 2012; Qi et al., 2018; Zhuang et al., 2017). This paradox illustrates how anthropogenic activities can both mitigate and trigger geomorphic hazards, underscoring the need for proactive management. Remote sensing and in-situ geodetic tools (e.g., He et al., 2020) should be deployed to monitor evolving instability, especially as warning systems remain limited in this rapidly urbanized region.

### 5.3. Short-term stage water height and infiltration

Comparison between pre- and post-construction topography derived stage water height and infiltration suggests that the city construction has modulated the landscape's response to storms (Figs. 7 and 8). Simulated storm precipitations based on 2013 observations spanning the rainy season are higher than the infiltration capacity of the soil and resulted in rapid increase in stage water height and infiltration after the storms (Fig. 8). Previous hydrological models suggested that the water infiltration in the loess slopes is less than 4 m (Wang et al., 2018; Zhuang et al., 2017). In contrast, our modeled results of an infiltration of 0.4 m at the outlet of the new urban region catchment are less than the previous modeled results. Such discrepancy could be due to our uncalibrated model parameters. For example, the conductivity applied in the model is  $10^{-7}$ , as the average from observed loess conductivity in a wide range from  $10^{-9}$  to  $2 \times 10^{-5}$  m/s (Domenico and Schwartz, 1997). Furthermore, although consolidation of the filled loess may affect hydrological properties over time, this effect is considered secondary within the scope of our modeling. Our primary objective is to assess natural geomorphic and hydrologic responses to post-construction topography, rather than simulate subsurface changes due to compaction. Additionally, because this anthropogenically altered landscape has no close analogs, modeling provides a valuable tool for exploring its large-scale environmental impacts.

Another factor controlling the modeled stage water height and infiltration is the prescribed local rainfall intensity. Currently, the 2013 rainfall record in Yan'an is used to generate monthly storm sequences,

representing short-term variability of rainfall events. Extremely long wet spells and rainfall intensification have been reported in Yan'an region (Miao et al., 2020) and around the world (Blöschl et al., 2020). The ongoing and future climate change due to global warming may increase the intensity, frequency, and duration of extreme precipitation events (Fischer et al., 2013; Fischer and Knutti, 2015; Orlowsky and Seneviratne, 2012), which could further modulate the post-MECC hydrological system of Yanhe River.

It is important to clarify that the modeling framework used in this study does not attempt to simulate future anthropogenic activities such as additional excavation, land use changes, or infrastructure expansion. Instead, our analysis focuses on projecting how natural surface processes, namely, overland flow, infiltration, erosion, and landsliding, respond to a landscape that has already been significantly altered by anthropogenic forces. The post-MECC topography, derived from high-resolution DEM data, embeds the direct effects of engineered terrain reshaping, including cut slopes, filled valleys, and regraded surfaces. These artificial landforms influence the hydrological pathways, slope geometry, and material properties in ways that diverge from natural loess hillslopes. Thus, while the model simulates natural processes, it does so over a terrain fundamentally restructured by human intervention. This approach allows us to assess the geomorphic and hydrological consequences of large-scale terrain modification, providing insight into the stability and resilience of anthropogenically constructed environments under natural forcing.

### 5.4. Implications

#### 5.4.1. Implications for land use management

The future vegetation condition and its effect on soil evolution will be influenced by various anthropogenic and environmental factors. Shifts in vegetation coverage and land use have a pronounced impact on soil erosion rates. The modeled results indicate that vegetation coverage could impact long-term soil erosion following the MECC project, particularly in areas with low NDVI values, which tend to experience greater erosion (Figs. 2b & 5a). This underscores the need for sustained vegetation coverage to reduce soil loss and maintain landscape stability, especially in areas vulnerable to construction-induced erosion. Vegetating newly constructed areas is essential for land reclamation efforts. The Conversion of Cropland to Forest Program, widely implemented in northern China (including the Loess Plateau) from 1999 to 2008, demonstrated the effectiveness of such efforts. This initiative converted 15 million hectares of farmland and 17 million hectares of barren mountainous land into vegetated areas (Hu et al., 2021). In Yan'an, this program resulted in a modest increase in NDVI by 0.023 (He et al., 2020). Continued efforts to establish and maintain vegetation within the new urbanized regions of Yan'an are essential, particularly following the extensive land disturbance caused by mega-scale city construction projects.

Previous modeling efforts on post-mining landscapes suggest that erosion rates spike immediately following mining activities, then decrease rapidly over a few years, eventually approaching natural erosion rates on millennial timescales (e.g., Molliere et al., 2002; Hancock et al., 2015; Coulthard et al., 2012). Similarly, our model projects a decline in erosion rates over the long term (Fig. 9). Given this, it is crucial to establish a robust monitoring network to track erosional instability during the most vulnerable period, which spans the first few years to several decades following city construction. This is especially important along the Yanhe River tributary, where knickpoint headward retreat could encroach upon the newly urbanized regions (Fig. 10).

Additionally, it is essential to assess the potential for loess landslides and implement early warning systems to ensure sustainable urban development in Yan'an new urban areas. Given the scale of the project and its location on the Loess Plateau, understanding the interactions between loess erosion and gully stabilization is vital. This should include investigations into stage water levels, infiltration processes, and

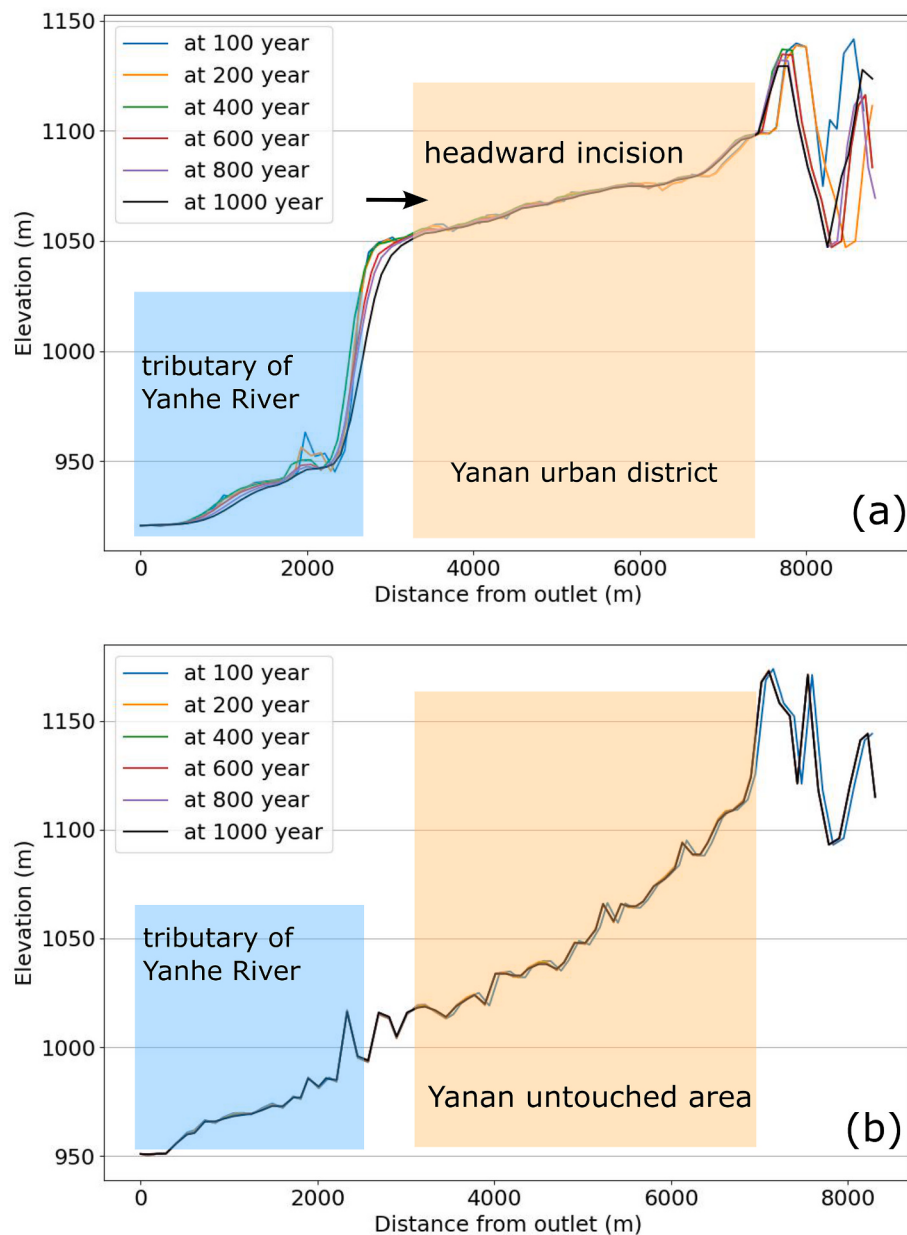


**Fig. 10.** Longitudinal profiles of the Yanhe River from north of the city new urban region to the outlet of catchment. (a) and (b) show the scenarios with and without the city construction respectively. In the former case, the knickpoint is retreating headward through time, incising the new urban region. The shadow regions represent the locations of Yan'an new urban region and tributary of Yanhe River, respectively.

mechanisms of seepage erosion in loess terrain (Juang et al., 2019). These assessments will play a critical role in minimizing the long-term impacts of erosion and ensuring the stability of the landscape.

The modeled short-term impacts on runoff and infiltration are informative for effective land use planning, particularly in the context of extreme weather events. The simulations suggest a higher water stage water level at the outlet of the Yanhe River tributary, implying a potential risk of flooding during heavy rainfall. Additionally, time series tests indicate that it takes significantly longer for stage height and infiltration to recover to baseline after such events. These insights can be useful for developing land use strategies that mitigate the risks of extreme weather, ensuring that urban development and agriculture do not exacerbate these effects. By incorporating these short-term predictions into planning, we can better adapt to the increasing frequency and intensity of extreme weather events.

#### 5.4.2. Implications for the landscape modeling field

This study contributes to landscape modeling by demonstrating the integration of post-transformation topography into physically based models. By using post-construction DEMs as fixed terrain input, we simulate natural processes such as erosion, overland flow, and landsliding on landscapes that have already been reshaped by anthropogenic transformations. This approach does not model the anthropogenic actions themselves but instead examines how natural processes operate within the constraints of engineered landforms (Valters, 2016; Harmon et al., 2019). Recent advancements in LEMs, such as Landlab, have enabled more accurate representation of dynamic terrain evolution over short to long timescales (Harmon et al., 2019). Our approach reinforces the importance of accounting for anthropogenic geometry (e.g., cut-fill patterns, slope regrading) when projecting natural processes, an area where most traditional models fall short. The study demonstrates how combining high-resolution terrain data with physics-based process modeling can provide useful insights into landscape stability in

urbanizing regions.

#### 5.4.3. Implications for understanding anthropogenic transformation and natural process interactions

This study contributes to a growing body of research on how large-scale anthropogenic terrain reshaping fundamentally alters Earth surface dynamics and interacts with natural geomorphic and hydrologic processes. Our findings emphasize that engineered topographies—such as those created by the MECC project—modify slope geometry, drainage pathways, soil properties, and vegetation distribution in ways that induce persistent feedbacks between human actions and natural landscape processes. This relation can amplify or dampen subsequent environmental responses, often with unintended consequences.

Such human–landscape feedbacks have been increasingly recognized in recent geomorphological literature as critical components of coupled socio-ecological systems (Chin et al., 2014). For instance, human decisions about land use and hazard mitigation can generate feedback loops that unintentionally increase landscape instability, as shown by post-fire sediment control strategies leading to accelerated channel incision (Chin et al., 2016). In our study, the anthropogenically altered terrain significantly increases landslide susceptibility at slope margins, underscoring how even stabilizing efforts (e.g., vegetation planting) must account for long-term feedbacks from slope hydrology and erosion processes.

Theoretical frameworks such as anthropogenic geomorphology emphasize the need to analyze both direct human actions and the cascading consequences of these activities across spatial scales and timeframes (Jefferson et al., 2013), along with legacy effects and cumulative alterations (Poeppl et al., 2017). These approaches align with our results, suggesting that future urbanization projects must account for the systemic and sometimes irreversible nature of terrain restructuring. The shift from viewing humans as external disturbance agents to embedded geomorphic actors capable of initiating feedback-rich, evolving landscapes is essential to advancing both theory and practice.

By applying numerical models over post-construction DEMs, this study highlights a practical method to explore the long-term effects of human-modified terrain on landscape evolution. This supports calls for integrated environmental modeling frameworks that bridge the gap between anthropogenic transformation and physical processes (Stephens et al., 2021). It also provides a valuable testbed for developing policies that promote sustainable urban expansion while anticipating emergent environmental risks.

#### 5.5. Model uncertainties and limitations

The sources of uncertainty in this model encompass parameters describing material properties, various rates, the model structure derived from governing equations, and the initial conditions of the model (e.g., Barnhart et al., 2020a). Calibration of the fluvial and diffusive models, along with parameterization, often relies on field sediment transport data collected over multiple years. Unfortunately, direct measurements of long-term rainfall, runoff, and sediment yield are unavailable in this region. To address this, sensitivity analysis in the forward model is applied to enhance projection fidelity (Atchley et al., 2019). For instance, our research considers a range of climate conditions and rainfall patterns (rainy and dry seasons). However, sensitivity analysis is not extended to some parameters that could influence the rate and pattern of post-MECC landscape evolution. Notably, sediment deposition is affected by slope and drainage area exponents ( $m$  and  $n$  in Eq. (2); Atchley et al., 2019), as advection-driven transport and slope sediment also modulate sediment deposition. Additionally, the diffusive property ( $d$  in Eq. (4)) impacts the amount of erosion and deposition. The variations in these parameters inevitably contribute to the increased uncertainty of the projected results.

Uncertainty arising from the model structure is not within the scope of this study. Barnhart et al. (2020a) proposed that models incorporating

various governing equations, such as the application of fluvial erosion thresholds and linear or non-linear hillslope transport, exhibit limited differences in erosion projections. Apart from the uncertainty associated with the model structure, exploring initial conditions is a primary focus of this study, aligning with the goal of assessing the impact of construction on landscape erosion. The initial conditions, extracted from pre- and post-construction topography, NDVI, and land use coverage, are adequate for the comparative analysis. These efforts in predicting model outcomes over timescales extending beyond the human lifespan remain crucial for sustainable development and environmental protection.

We acknowledge that the model used in this study (Landlab) includes simplifications that limit its ability to fully represent the complexity of anthropogenic terrain, such as engineered drainage systems, surface sealing, and fill heterogeneity. Landlab and similar LEMs are primarily designed to simulate natural surface processes such as erosion and deposition on geologically controlled landscapes (Hobley et al., 2017; Barnhart et al., 2020a). However, rather than simulating future anthropogenic activities directly, our focus is on understanding how natural processes—such as erosion, infiltration, and slope failure—respond to anthropogenic topographic changes already present in the post-MECC DEM. This approach follows prior applications of LEMs to post-mining landscapes, landfills, and tailing dams where artificial topography is used as the starting condition (Neuhold and Nachtnebel, 2011; Hancock et al., 2015; Slingerland et al., 2018).

Thus, while the processes are natural, their triggers and spatial configurations are shaped by human-induced alterations. We argue that this distinction allows the model to remain scientifically valid for evaluating post-construction geomorphic risks, even if it does not incorporate all engineered controls. In this way, our study builds on efforts to extend LEM applications to semi-urban or regraded terrains (e.g., Reed and Kite, 2020). Future work could improve realism by incorporating anthropogenic surface properties, soil treatments, and hydrologic infrastructure—such as culverts or sealed drainage—supported by field surveys, high-resolution DEMs, or municipal planning data (e.g., Hogue et al., 2013; Li et al., 2023).

In the context of the long-term projection and simulation conducted herein, it is assumed that no artificial interventions, such as soil stabilization techniques, stormwater runoff sewers, or paved surfaces, will be constructed or implemented to alter the natural runoff patterns within the studied area over the next one hundred years. However, based on satellite imagery and InSAR data (e.g. Pu et al., 2023), discernible indications suggest the implementation of slope stabilization measures along the margins of the city. Furthermore, creep tests on soil samples suggested a progressively diminishing rate of deformation after MECC projects (Hou et al., 2023). These measures manifest in the form of constructed walls and strategic vegetation planting, ostensibly serving to mitigate potential soil erosion and slope instability within the landscape under scrutiny. Meanwhile, vegetation restoration in Yan'an new urban area has been reported (e.g., Xu et al., 2019). Although these elements are not explicitly modeled in our current LEM framework, they represent real-world controls that could be incorporated in future coupled models integrating anthropogenic infrastructure. Such observations underscore the nuanced interplay between natural topography and anthropogenic interventions, warranting further investigation into their efficacy and implications within the broader geoscientific discourse.

Meanwhile, several geological processes are simplified to enhance the model's clarity and efficiency. Our approach does not account for soil profile characteristics, including eolian effects, chemical weathering of the soil, and the relationship between infiltration and landslides. Additionally, the 90 m DEM resolution is relatively coarse, potentially leading to the loss of fine-scale details in the landform. The chosen DEM represents a compromise balancing spatial extent, catchment resolution, model runtime, and product availability both pre- and post-construction. Consequently, beyond developing numerical methods,

obtaining a recent, high-resolution DEM becomes imperative to elucidate morphological details post-city construction. We assume that subsidence resulting from soil consolidation has a limited impact on the DEM, a premise supported by studies in surface deformation analysis using Synthetic Aperture Radar imagery (e.g., Hu et al., 2021; Pu et al., 2023; Zhou et al., 2022). These studies indicate decelerated subsidence rates, decreasing from 70 mm yr<sup>-1</sup> during 2014–2020 to a near stabilization within about a decade.

## 6. Conclusions

Landscape evolution models provide a means to quantitatively simulate how natural processes evolve on landforms permanently reshaped by anthropogenic transformations. In this study, we integrate LEM Landlab and its components to assess erosion patterns, soil depth, and landslide failure probability following a 100-year simulation of a mega-scale anthropogenic topography on the Loess Plateau of China. A comparison between pre- and post-city construction modeled results reveals a significant increase in soil erosion and a substantial decrease in soil depth, exceeding the scenario without city construction by an order of magnitude, if no human intervention/mitigation. The most pronounced erosion and a heightened risk of slope failures occur at the margins of the new urban, characterized by steep slopes and gullies. Additionally, we investigate short-term impacts on the stage water height and infiltration. During rainy-season storms, stage water height and infiltration are influenced by the construction. The insights derived from these modeled results advance understanding how human activities affect erosional stability and river evolution across various time-scales, aiding in the mitigation of geohazards in this fragile loess environment.

## Declaration of competing interest

We certify that they have no affiliations with or involvement in any organization or entity with any financial interest or non-financial interest in the subject matter or materials discussed in this manuscript.

## Acknowledgments

The landscape evolution code, Landlab and its libraries are available on Landlab webpage (<https://landlab.readthedocs.io/en/latest/>) and Zenodo (<https://doi.org/10.5281/zenodo.595872>). The in-situ precipitation data of 2013 is available in Supplementary materials. The land use data is extracted in 2010 and 2020 as pre- and post-construction data from GlobeLand30 ([www.globallandcover.com](http://www.globallandcover.com)). NDVI data from NASA MODIS product MOD13Q1 in 2018 and 2011 (<https://doi.org/10.5067/MODIS/MOD13Q1.061>). The DEM data from TanDEM-X DEM and Shuttle Radar Topography Mission from opentopography ([opentopography.org](http://opentopography.org)). L.X. thanks Christopher Scholz and Katherine Barnhart for helpful communication and suggestions. X.H. was supported by the National Natural Science Foundation of China (42371078). Q.T. was supported by the National Natural Science Foundation of China (U2243226). We thank editor and reviewers for their suggestions.

## Appendix A. Supplementary data

Supplementary data to this article can be found online at <https://doi.org/10.1016/j.geomorph.2025.109976>.

## Data availability

No data was used for the research described in the article.

## References

- Alexandridis, T.K., Sotiropoulou, A.M., Bilas, G., Karapetsas, N., Silleos, N.G., 2015. The effects of seasonality in estimating the C-factor of soil erosion studies. *Land Degrad. Dev.* 26 (6), 596–603.
- Allan, A., Soltani, A., Abdi, M.H., Zarei, M., 2022. Driving forces behind land use and land cover change: a systematic and bibliometric review. *Land* 11 (8), 1222.
- Atchley, A.L., Birdsall, K.H., Crowell, K., Middleton, R.S., Stauffer, P.H., 2019. Simulating 10,000 years of erosion to assess nuclear waste repository performance. *Geosciences* 9 (3), 120.
- Barnhart, K.R., Tucker, G.E., Doty, S.G., Glade, R.C., Shobe, C.M., Rossi, M.W., Hill, M.C., 2020a. Projections of landscape evolution on a 10,000 year timescale with assessment and partitioning of uncertainty sources. *J. Geophys. Res. Earth* 125 (12), e2020JF005795.
- Barnhart, K.R., Hutton, E.W., Tucker, G.E., Gasparini, N.M., Istanbulluoglu, E., Hobley, D.E., Bandaragoda, C., 2020b. Landlab v2.0: a software package for Earth surface dynamics. *Earth Surf. Dyn.* 8 (2), 379–397.
- Blöschl, G., Kiss, A., Viglione, A., Barriendos, M., Böhm, O., Brázdil, R., Wetter, O., 2020. Current European flood-rich period exceptional compared with past 500 years. *Nature* 583 (7817), 560–566.
- Campforts, B., Overeem, I., Gasparini, N., Piper, M., Arthurs, L., 2021. Modeling earth surface processes for the future: ESPin, a summer school focusing on cyber training and professional networking. In: AGU Fall Meeting Abstracts, vol. 2021 (ED55C-0300 pp., December).
- Cao, Z., Han, Z., Li, Y., Wang, J., 2024. Distribution of topographical changes triggered by prolonged heavy rainfall in the Chinese Loess Plateau: a case study of the Gutun catchment in Yan'an. *J. Geogr.* 34 (3), 571–590.
- Chen, X., Yu, Y., Chen, J., Zhang, T., Li, Z., 2016. Seasonal and interannual variation of radiation and energy fluxes over a rain-fed cropland in the semi-arid area of Loess Plateau, northwestern China. *Atmos. Res.* 176, 240–253.
- Chen, H., Wang, X., Lu, H., Van Balen, R., 2021. Anthropogenic impacts on Holocene fluvial dynamics in the Chinese Loess Plateau, an evaluation based on landscape evolution modeling. *Geomorphology* 392, 107935.
- Chin, A., Florsheim, J.L., Wohl, E., Collins, B.D., 2014. Feedbacks in human–landscape systems. *Environ. Manag.* 53 (1), 28–41.
- Chin, A., An, L., Florsheim, J.L., Laurencio, L.R., Marston, R.A., Solverson, A.P., Wohl, E., 2016. Investigating feedbacks in human–landscape systems: lessons following a wildfire in Colorado, USA. *Geomorphology* 252, 40–50.
- Collins, M., et al., 2013. Long-term climate change: projections, commitments and irreversibility. In: Stocker, T.F., Qin, D., Plattner, G.-K., Tignor, M., Allen, S.K., Boschung, J., Nauels, A., Xia, Y., Bex, V., Midgley, P.M. (Eds.), *Climate Change 2013: The Physical Science Basis, Contribution of Working Group I to the Fifth Assessment Report of the Intergovernmental Panel on Climate Change*. Cambridge University Press, Cambridge, United Kingdom and New York, NY, USA, pp. 1029–1136. <https://doi.org/10.1017/cbo9781107415324.024>.
- Cossart, E., Fressard, M., Chaize, B., 2020. Spatial patterns of vineyard landscape evolution and their impacts on erosion susceptibility: RUSLE simulation applied in Mercurey (Burgundy, France) since the mid-20th century. *Erdkunde H* 4, 281–300.
- Coulthard, T.J., Hancock, G.R., Lowry, J.B., 2012. Modelling soil erosion with a downscaled landscape evolution model. *Earth Surf. Process. Landf.* 37 (10), 1046–1055.
- Davy, P., Lague, D., 2009. Fluvial erosion/transport equation of landscape evolution models revisited. *J. Geophys. Res. Earth* 114 (F3).
- Derbyshire, E., Meng, X., Dijkstra, T.A. (Eds.), 2000. *Landslides in the Thick Loess Terrain of North-West China*. Wiley-Blackwell.
- Domenico, P.A., Schwartz, F.W., 1997. *Physical and Chemical Hydrogeology*. John Wiley & Sons.
- Duzant, J.H., Morgan, R.P.C., Wood, G.A., Deeks, L.K., 2011. Modelling the role of vegetated buffer strips in reducing transfer of sediment from land to watercourses. In: *Handbook of Erosion Modelling*, pp. 249–262.
- Ehrlich, P.R., Holdren, J.P., 1971. Impact of population growth: complacency concerning this component of man's predicament is unjustified and counterproductive. *Science* 171 (3977), 1212–1217.
- Ellis, E.C., Kaplan, J.O., Fuller, D.Q., Vavrus, S., Goldeijk, K.K., Verburg, P.H., 2013. Used planet: a global history. *Proc. Natl. Acad. Sci. USA* 110 (20), 7978–7985.
- Fischer, E.M., Knutti, R., 2015. Anthropogenic contribution to global occurrence of heavy-precipitation and high-temperature extremes. *Nat. Clim. Chang.* 5 (6), 560–564.
- Fischer, E.M., Beyerle, U., Knutti, R., 2013. Robust spatially aggregated projections of climate extremes. *Nat. Clim. Chang.* 3 (12), 1033–1038.
- Fu, B., Liu, Y., Lü, Y., He, C., Zeng, Y., Wu, B., 2011. Assessing the soil erosion control service of ecosystems change in the Loess Plateau of China. *Ecol. Complex.* 8 (4), 284–293.
- Green, W.H., Ampt, G.A., 1911. The flow of air and water through soils. *J. Agric. Sci.* 4, 1–24.
- Hammond, C., 1992. *Level I Stability Analysis (LISA) Documentation for Version 2.0*, vol. 285. US Department of Agriculture, Forest Service, Intermountain Research Station.
- Hancock, G.R., Lowry, J.B.C., Coulthard, T.J., 2015. Catchment reconstruction—erosional stability at millennial time scales using landscape evolution models. *Geomorphology* 231, 15–27.
- Hancock, G.R., Lowry, J.B.C., Saynor, M., 2017. Surface armour and erosion–impacts on long-term landscape evolution. *Land Degrad. Dev.* 28 (7), 2121–2136.
- Harmon, B.A., Mitasova, H., Petrasova, A., Petras, V., 2019. r. sim. terrain 1.0: a landscape evolution model with dynamic hydrology. *Geosci. Model Dev.* 12 (7), 2837–2854.

- He, M.N., Wang, Y.Q., Tong, Y.P., Zhao, Y.L., Qiang, X.K., Song, Y.G., Wang, L., Song, Y., Wang, G.D., He, C.X., 2020. Evaluation of the environmental effects of intensive land consolidation: a field-based case study of the Chinese Loess Plateau. *Land Use Policy* 94, 104523.
- Hobley, D.E., Adams, J.M., Nudurupati, S.S., Hutton, E.W., Gasparini, N.M., İstanbulluoglu, E., Tucker, G.E., 2017. Creative computing with Landlab: an open-source toolkit for building, coupling, and exploring two-dimensional numerical models of Earth-surface dynamics. *Earth Surf. Dyn.* 5 (1), 21–46.
- Hogue, T.S., et al., 2013. Urban infrastructure influences on runoff and pollution. *J. Hydrol.* 485, 177–190.
- Hou, K., Li, X., Wang, J., Zhang, J., 2016. Evaluating Ecological Vulnerability Using the GIS and Analytic Hierarchy Process (AHP) Method in Yan'an, China. *Pol. J. Environ. Stud.* 25 (2).
- Hou, X., Qi, S., Yu, Y., Zheng, J., 2023. Long-term settlement characterization of high-filling foundation in the mountain excavation and city construction area of the Yan'an new district, China. *J. Earth Sci.* 34 (6), 1908–1915.
- Hu, X., Xue, L., Yu, Y., Guo, S., Cui, Y., Li, Y., Qi, S., 2021. Remote sensing characterization of mountain excavation and city construction in Loess Plateau. *Geophys. Res. Lett.* 48 (21), e2021GL095230.
- Huo, A., Yang, L., Peng, J., Cheng, Y., Jiang, C., 2020. Spatial characteristics of the rainfall induced landslides in the Chinese Loess Plateau. *Hum. Ecol. Risk Assess. Int.* 26 (9), 2462–2477.
- Hutton, E., Barnhart, K., Hobley, D., Tucker, G., Nudurupati, S., Adams, J., Gasparini, N., Shobe, C., Strauch, R., Knuth, J., Mouchene, M., Lyons, N., Litwin, D., Glade, R., 2020. Giuseppicoppola95. In: Manaster, A., Abby, L., Thyng, K., Rengers, F. (Eds.), *Landlab [Computer Software]*. <https://doi.org/10.5281/zenodo.595872>.
- Jefferson, A.J., Wegmann, K.W., Chin, A., 2013. Geomorphology of the Anthropocene: understanding the surficial legacy of past and present human activities. *Anthropocene* 2, 1–3.
- Juang, C.H., Dijkstra, T., Wasowski, J., Meng, X., 2019. Loess geohazards research in China: advances and challenges for mega engineering projects. *Eng. Geol.* 251, 1–10.
- Keles, F., Nefeslioglu, H.A., 2021. Infinite slope stability model and steady-state hydrology-based shallow landslide susceptibility evaluations: the Guneysu catchment area (Rize, Turkey). *CATENA* 200, 105161.
- Kou, P., Xu, Q., Yunus, A.P., Liu, J., Xu, Y., Wang, C., Dong, X., 2020. Landslide-controlled soil erosion rate in the largest tableland on the Loess Plateau, China. *Hum. Ecol. Risk Assess. Int.* 26 (9), 2478–2499.
- Lambin, E.F., Geist, H.J., Lepers, E., 2003. Dynamics of land-use and land-cover change in tropical regions. *Annu. Rev. Environ. Resour.* 28 (1), 205–241.
- Leng, Y.-q., Lyu, Y., He, M., Zhao, J., 2023. Geoheritage sites of Yan'an City for geotourism in China's Middle Loess Plateau. *Geoheritage* 15 (1), 1–13.
- Li, G., Sheng, L., 2011. Model of water-sediment regulation in Yellow River and its effect. *SCIENCE CHINA Technol. Sci.* 54 (4), 924–930.
- Li, S., Wang, T., Yan, C., 2017. Assessing the role of policies on land-use/cover change from 1965 to 2015 in the Mu Us Sandy Land, northern China. *Sustainability* 9 (7), 1164.
- Li, G., Wang, F., Ma, W., Fortier, R., Mu, Y., Mao, Y., Hou, X., 2018a. Variations in strength and deformation of compacted loess exposed to wetting-drying and freeze-thaw cycles. *Cold Reg. Sci. Technol.* 151, 159–167.
- Li, Y., Zhang, T., Zhang, Y., Xu, Q., 2018b. Geometrical appearance and spatial arrangement of structural blocks of the Malan loess in NW China: implications for the formation of loess columns. *J. Asian Earth Sci.* 158, 18–28.
- Li, S., et al., 2023. Integrated urban flood modeling with DEMs and drainage infrastructure data. *Environ. Model. Softw.* 166, 105610.
- Liu, T.S., Zhang, S., Han, J.M., 1987. Stratigraphy and palaeoenvironmental changes in the loess of Central China. *Quat. Sci. Rev.* 6, 489–501.
- Liu, X., Zhao, C., Zhang, Q., Yang, C., Zhu, W., 2020. Heifangtai loess landslide type and failure mode analysis with ascending and descending Spot-mode TerraSAR-X datasets. *Landslides* 17 (1), 205–215.
- Ma, L., Qi, S., Zheng, B., Guo, S., Huang, Q., Yu, X., 2020. Farming influence on physical-mechanical properties and microstructural characteristics of backfilled loess farmland in Yan'an, China. *Sustainability* 12 (14), 5516.
- Maurer, T., Gerke, H.H., 2016. Processes and modeling of initial soil and landscape development: a review. *Vadose Zone J.* 15 (12), 1–20. <https://doi.org/10.2136/vzj2016.05.0048>.
- Meng, Q., Li, W., Raspini, F., Xu, Q., Peng, Y., Ju, Y., Casagli, N., 2021. Time-series analysis of the evolution of large-scale loess landslides using InSAR and UAV photogrammetry techniques: a case study in Hongheyan, Gansu Province, Northwest China. *Landslides* 18 (1), 251–265.
- Miao, C., Zheng, H., Jiao, J., Feng, X., Duan, Q., Mpofu, E., 2020. The changing relationship between rainfall and surface runoff on the Loess Plateau, China. *J. Geophys. Res. Atmos.* 125 (8), e2019JD032053.
- Moliere, D.R., Evans, K.G., Willgoose, G.R., 2002. Temporal Trends in Erosion and Hydrology for a Post-mining Landform at Ranger Mine, vol. 31. Research Institute.
- Moore, J.W. (Ed.), 2016. Anthropocene or Capitalocene?: Nature, History, and the Crisis of Capitalism. Pm Press.
- Neuhold, C., Nachtnebel, H.P., 2011. Assessing flood risk associated with waste disposals: methodology, application and uncertainties. *Nat. Hazards* 56 (1), 359–370.
- Orłowsky, B., Seneviratne, S.I., 2012. Global changes in extreme events: regional and seasonal dimension. *Clim. Chang.* 110, 669–696.
- Panagos, P., Borrelli, P., Meusburger, K., Alewell, C., Lugato, E., Montanarella, L., 2015. Estimating the soil erosion cover-management factor at the European scale. *Land Use Policy* 48, 38–50.
- Peleg, N., Fatichi, S., Paschalis, A., Molnar, P., Burlando, P., 2017. An advanced stochastic weather generator for simulating 2-D high-resolution climate variables. *J. Adv. Model. Earth Syst.* 9 (3), 1595–1627.
- Poeppl, R.E., Keesstra, S.D., Maroulis, J., 2017. A conceptual connectivity framework for understanding geomorphic change in human-impacted fluvial systems. *Geomorphology* 277, 237–250.
- Pu, C., Xu, Q., Wang, X., Li, Z., Chen, W., Zhao, K., Liu, J., 2023. Refined mapping and kinematic trend assessment of potential landslides associated with large-scale land creation projects with multitemporal InSAR. *Int. J. Appl. Earth Obs. Geoinf.* 118, 103266.
- Qi, X., Xu, Q., Liu, F., 2018. Analysis of retrogressive loess flowslides in Heifangtai, China. *Eng. Geol.* 236, 119–128.
- Rawls, W.J., Ahuja, L.R., Brakensiek, D.L., Shirmohammadi, A., 1992. *Infiltration and Soil Water Movement*. McGraw-Hill Inc., pp. 5–51.
- Reed, M., Kite, S., 2020. Peripheral gully and landslide erosion on an extreme anthropogenic landscape produced by mountaintop removal coal mining. *Earth Surf. Process. Landf.* 45 (9), 2078–2090.
- Rengers, F.K., McGuire, L.A., Kean, J.W., Staley, D.M., Hobley, D., 2016. Model simulations of flood and debris flow timing in steep catchments after wildfire. *Water Resour. Res.* 52, 6041–6061.
- Shobe, C.M., Tucker, G.E., Barnhart, K.R., 2017. The SPACE 1.0 model: a Landlab component for 2-D calculation of sediment transport, bedrock erosion, and landscape evolution. *Geosci. Model Dev.* 10 (12), 4577–4604.
- Singer, M.B., Michaelides, K., Hobley, D.E., 2018. STORM 1.0: a simple, flexible, and parsimonious stochastic rainfall generator for simulating climate and climate change. *Geosci. Model Dev.* 11 (9), 3713–3726.
- Slingerland, N., Isidoro, A., Fernandez, S., Beier, N.A., 2018. Geomorphic analysis for tailings dam design in consideration of a 1000-year closure design life. In: *Proceedings of the 2nd International Congress on Planning for Closure of Mining Operations*, pp. 1–9.
- Stephens, C.M., Lall, U., Johnson, F.M., Marshall, L.A., 2021. Landscape changes and their hydrologic effects: interactions and feedbacks across scales. *Earth Sci. Rev.* 212, 103466.
- Strauch, R., İstanbulluoglu, E., Nudurupati, S.S., Bandaragoda, C., Gasparini, N.M., Tucker, G.E., 2018. A hydroclimatological approach to predicting regional landslide probability using Landlab. *Earth Surf. Dyn.* 6 (1), 49–75.
- Tabarsa, A., Latifi, N., Meehan, C.L., Mahniloh, K.N., 2018. Laboratory investigation and field evaluation of loess improvement using nanoclay—a sustainable material for construction. *Constr. Build. Mater.* 158, 454–463.
- Valters, D., 2016. Modelling geomorphic systems: landscape evolution. In: *Geomorphological Techniques*. British Society for Geomorphology.
- Wang, T., Wu, J., Kou, X., Oliver, C., Mou, P., Ge, J., 2010. Ecologically asynchronous agricultural practice erodes sustainability of the Loess Plateau of China. *Ecol. Appl.* 20 (4), 1126–1135.
- Wang, G., Li, T., Xing, X., Zou, Y., 2015. Research on loess flow-slides induced by rainfall in July 2013 in Yan'an, NW China. *Environ. Earth Sci.* 73 (12), 7933–7944.
- Wang, W., Wang, Y., Sun, Q., Zhang, M., Qiang, Y., Liu, M., 2018. Spatial variation of saturated hydraulic conductivity of a loess slope in the South Jingyang Plateau, China. *Eng. Geol.* 236, 70–78.
- Wang, J., Zhang, D., Wang, N., Gu, T., 2019. Mechanisms of wetting-induced loess slope failures. *Landslides* 16, 937–953.
- Wei, Y., Liu, X., Zhao, C., Tomás, R., Jiang, Z., 2021. Observation of surface displacement associated with rapid urbanization and land creation in Lanzhou, Loess Plateau of China with Sentinel-1 SAR imagery. *Remote Sens.* 13 (17), 3472.
- Whipple, K.X., Tucker, G.E., 1999. Dynamics of the stream-power river incision model: implications for height limits of mountain ranges, landscape response timescales, and research needs. *J. Geophys. Res. Solid Earth* 104 (B8), 17661–17674.
- Wu, Q., Jia, C., Chen, S., Li, H., 2019. Sbas-insar based deformation detection of urban land, created from mega-scale mountain excavating and valley filling in the Loess Plateau: the case study of Yan'an City. *Remote Sens.* 11 (14), 1673.
- Xu, L., Qiao, X., Wu, C., Iqbal, J., Dai, F., 2012. Causes of landslide recurrence in a loess platform with respect to hydrological processes. *Nat. Hazards* 64 (2), 1657–1670.
- Xu, R., Li, X., Yang, W., Jiang, C., Rabiei, M., 2019. Use of local plants for ecological restoration and slope stability: a possible application in Yan'an, Loess Plateau, China. *Geomat. Nat. Haz. Risk* 10 (1), 2106–2128.
- Yang, H., Xie, W.L., Liu, Q.Q., Zhu, R.S., Liu, Y.Y., 2022. Three-stage collapsibility evolution of Malan loess in the Loess Plateau. *Catena* 217, 106482.
- Zeng, L., Huang, Y.H., 2010. Valley evolution and geologic hazard occurrences in the Loess Plateau of China-a case study: Zichang County in the northern Loess Plateau of Shaanxi Province. *Chin. J. Geol. Hazard Control* 21 (3), 67–72.
- Zhao, G., Mu, X., Wen, Z., Wang, F., Gao, P., 2013. Soil erosion, conservation, and environment changes in the Loess Plateau of China. *Land Degrad. Dev.* 24 (5), 499–510.
- Zhou, C., Lan, H., Bürgmann, R., Warner, T.A., Clague, J.J., Li, L., Yao, J., 2022. Application of an improved multi-temporal InSAR method and forward geophysical model to document subsidence and rebound of the Chinese Loess Plateau following land reclamation in the Yan'an New District. *Remote Sens. Environ.* 279, 113102.
- Zhu, Y., Jia, X., Shao, M., 2018. Loess thickness variations across the Loess Plateau of China. *Surv. Geophys.* 39 (4), 715–727.
- Zhuang, J., Peng, J., Wang, G., Iqbal, J., Wang, Y., Li, W., Zhu, X., 2017. Prediction of rainfall-induced shallow landslides in the Loess Plateau, Yan'an, China, using the TRIGRS model. *Earth Surf. Process. Landf.* 42 (6), 915–927.